Department of Mechanical Engineering

Energy Systems Research Unit

MARINE CURRENT TURBINES: ARRAY EFFECTS

Author: Miguel Gallego Gómez
Supervisor: Dr Andrew Grant

MSc in Energy Systems and the Environment

September 2008

COPYRIGHT DECLARATION

ACKNOWLEDGEMENTS

I would like to show my gratitude to Dr Andy Grant for his support, guidance and invaluable advice all throughout the project, and to Dr Gary Connor, for his commitment and his help.

I would also like to thank Pat McGuiness and John Redgate for the support with the electrical system; Jim Doherty, Neil McGrindle, Martin Rooney and Ronnie McKenzie for the manufacturing of the models; Tom McCombes for the designing of the 3D graphs and John Carlin and Derek McNee for his support in the hydrodynamics lab.

ABSTRACT

As marine current turbines become more widely used, and their role within the renewable energies gets a higher priority in the future UK Government's energy plans, it is necessary to achieve a better understanding of this technology for it to be smoothly introduced into the energy sector.

The only way marine current turbines can be connected into the grid and make some significant contribution to requirements is being part of a farm. Because of this, and in the same way that was done with wind turbines when they were starting to show their now undeniable potential, it is necessary to study, simulate and understand the interactions between marine current turbines when they are deployed in the form of an array. This project tried to clarify to a modest extent how a turbine interacts with the other devices surrounding it.

Real physical small scale models of a horizontal axis marine current turbine were designed to behave as closely as possible to a real machine, and an electrical system was designed for the whole assembly to simulate the way a real marine current turbine would be producing energy in a full scale array on a real site. The array was tested inside a flume for different configurations, with a range of different loading ratios for the turbines, trying to simulate how a real grid-connected array might have demand fluctuations and hence different power outputs.

The performance of the turbines was analyzed focusing on their power output, and wake and blockage effect analysis were carried out based on the flow speed measurements taken.

Findings showed the importance of the different configurations when trying to optimize an array, examined the interactions between array configuration and the loading ratios of the turbines, and revealed the clear impact of the array effects on the overall power output.

CONTENTS

1. TIDAL STREAM ENERGY

1.1. THE TIDES

The tides are the cyclic movements of the Earth's masses of water due to the tidal forces created by the relative motion of the Sun-Earth-Moon system. This movements change the level of the ocean in the coast creating cyclic flows known as tidal currents.

The Sun and the Moon interact with the Earth via gravitational forces, and depending on their position they produce different types of tides. When the Sun and the Moon separated by 90º when viewed from the Earth (Moon at first quarter or third quarter), the gravitational forces of both heavenly bodies produce the neap tides, when the tidal range is minimum, and when the Moon is aligned with the Sun (new and full moon), the gravitational forces of both bodies align producing the spring tides, with the maximum tidal range and hence the strongest tidal currents.

This interaction is schematically shown in figure 1 below:

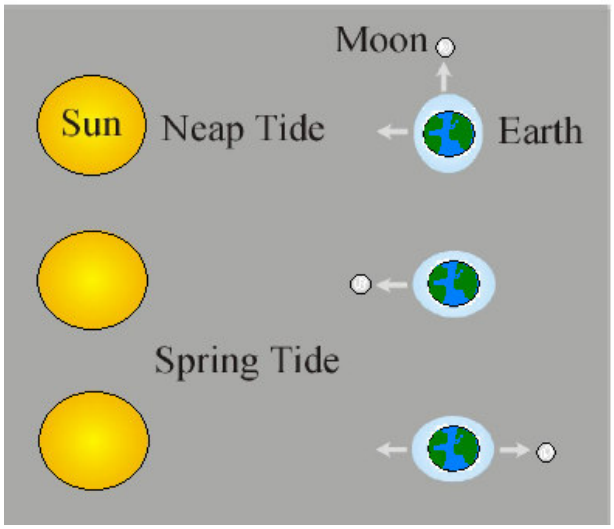

Figure 1. Astral gravitational influence on the tides [17].

Although tidal currents are quite complex, they can be scheduled. Tides are semidiurnal in most of the places, with two high tides or floods (when the flow goes in), and two low tides or ebbs (when the flow goes out) every 24 hours.

1.2. THE SITES

The magnitude of a tide in a specific location is highly depending on the shape of both the sea bed and the coast line. Tidal currents are then stronger in very specific places, such as estuaries, where the narrowness of the cross-sectional are of the flow increases the velocity of the water flow, or straits, where the flow is constrained between either main lands or land and islands.

The typical site where tidal currents would be suitable for energy harnessing would then be the channels appearing in the locations previously mentioned, with a cross-sectional area that changes all along the channel, delimited by the sea bed, the channels sides and the water surface.

The typical appearance of these channels is shown in figure 2 below:

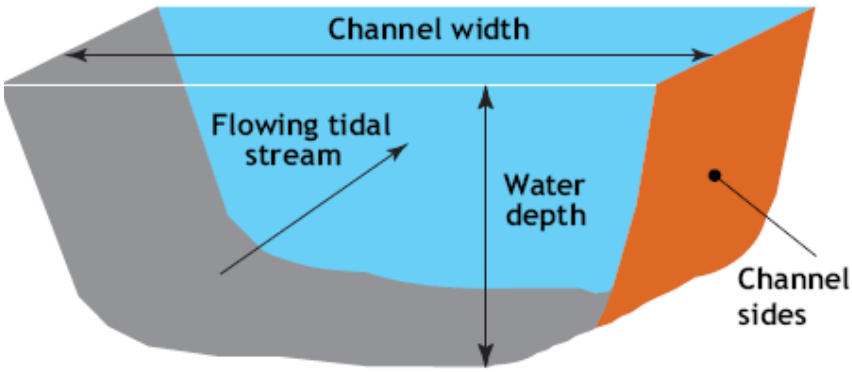

Figure 2. Appearance of a marine current turbine site.[16]

Due to the many differences between each site due to the shape of the channels and the surroundings, tidal currents are subject to local variations. Therefore, specific environmental studies and bathymetry analysis are required, with the water depth and the speed of the tidal currents - usually characterized by the velocity of both the spring and the neap tide – being the main parameters dictating the viability of a site.

1.2.1. UK sites

The map showing the tidal resource around the UK in terms of peak flow speeds for spring tides is shown in figure 3 below:

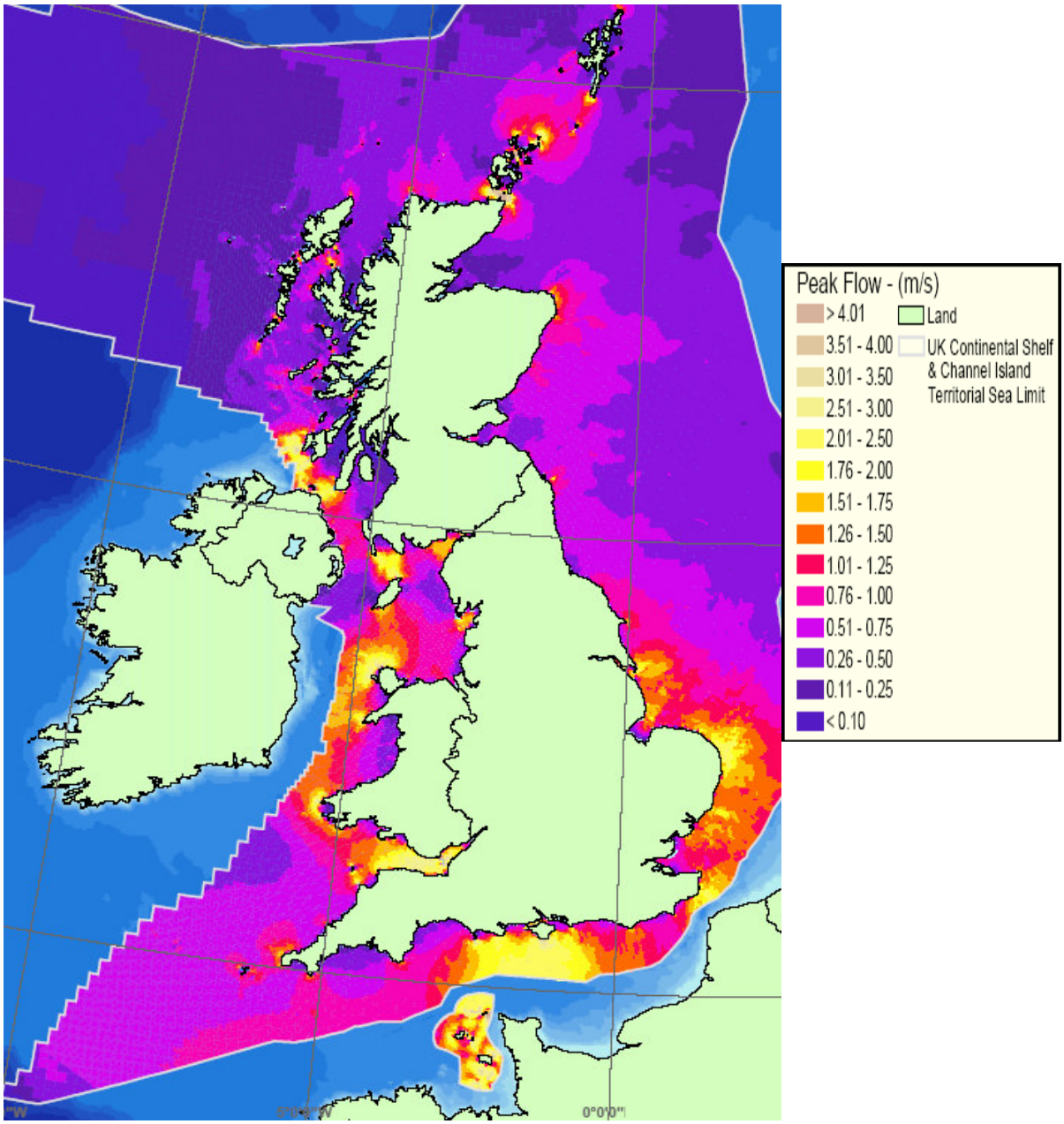

Figure 3. UK peak flow speeds for a spring tide [18]

As it can be seen in map, the potential for this source of energy in the UK is quite significant, and considering devices with a cut-in speed and a rated speed of 0.75 and

2 m/s respectively, the number of sites which could be actually suitable for energy production is quite numerous.

A summary of the most interesting sites in terms of extractable and available energy (accounting for 80% of the total UK resource) is detailed in table 1 below, together with their individual contribution to the UK resource [12]:

Site	Energy [GWh/year]	Contribution [%]
Pentland Skerries	3901	17.9
Stroma, Pentland Firth	2774	12.7
Duncansby Head, Pentland Firth	2031	9.3
Casquets, Channel Islands	1651	7.6
S. Ronaldsay, Pentland Firth	1518	7.0
Hoy, Pentland Firth	1377	6.3
Race of Alderney, Channel Islands	1365	6.3
S. Ronaldsay, Pentland Skerries	1147	5.3
Rathlin Island	866	4.0
Mull of Galloway	806	3.7

Table 1. Main UK sites.

1.3. THEORY REVIEW

1.3.1. Fluid dynamics

Marine current turbines use the tidal currents to produce energy. They are built with hydrofoil section blades. When this blades are set with a positive angle of attack (right drawing in figure 4 below) against an incoming flow (blue arrow), the flow covers the up and down contours of the blade with different speeds, creating a drag force (red arrow) and a difference in the pressure distribution (green lines) which creates a lift force (green arrow) pulling the blade.

This forces distribute along the blade and have opposite directions in each blade (assuming the turbine consist of two blades) creating a resulting torque.

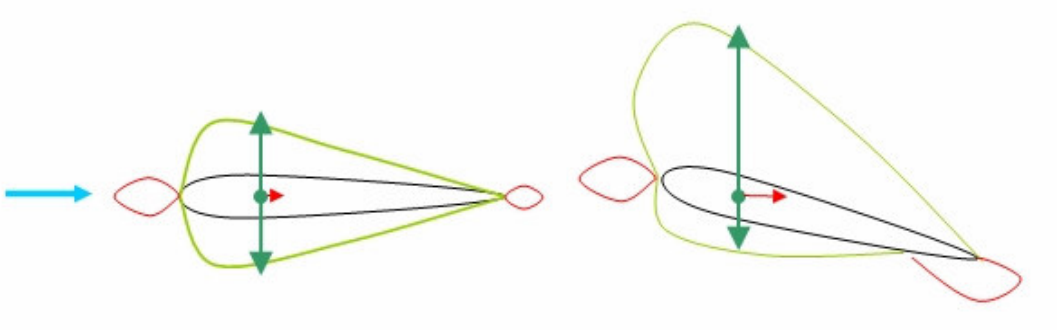

Figure 4. Pressure distribution and resultant forces through a hydrofoil section. [11]

1.3.2. Betz's Law

Marine current turbines extract kinetic energy from a moving flow, therefore they are subject to the Betz's Law.

The power in a cylinder of moving fluid is given by the following expression:

$$P = \frac{1}{2}\rho A V^3$$

Where A is the section of the cylinder and V the average speed of the flow.

However, the Betz´s Law assumes the cross-sectional area of the flow upstream of the turbine to increase when approaching the device and once again when leaving the device, with the consequent pressure change, decreasing both the speed of the flow - to maintain continuity – and the linear momentum – as energy was extracted from the flow -.

Because of this, it can be shown that as the flow needs the necessary amount of energy to leave the rotor region, only a 59% of the total available energy in the flow can be extracted theoretically. This is known as the Betz´s Limit, and it applies to every free stream turbine operating in air or water. Furthermore, rotors have losses when operating, and hence coefficients of performance close to the Betz´s Limit (Cp = 0.593) have been impossible to reach so far.

1.3.3. Energy production

In those sites where flows are tidal induced, the velocity would be described by a sinusoidal pattern given by:

$$V = V_{max} \sin \omega t$$

With $\omega = 2\pi/T$, where T is the period of the tidal cycle, about 745 minutes. Marine current turbines are usually designed to produce energy in both directions of the flow, and the power output is meant to be the same in both of them. This power output given by:

$$P = C_p \frac{1}{2} \rho A_{rotor} V^3$$

Where C_p would be the coefficient of performance previously mentioned.

Marine current turbines start to produce energy when their cut-in speed is reached, and their output increases until the rated-power is reached. The inclusion of a cut-out speed depends on the characteristics of the site and it is not usually necessary due to the high predictability of tidal currents.

Figure 5 below shows the available (blue) and estimated energy over half a tidal cycle, with the energy produced at rated speed during one quarter of the cycle striped in green:

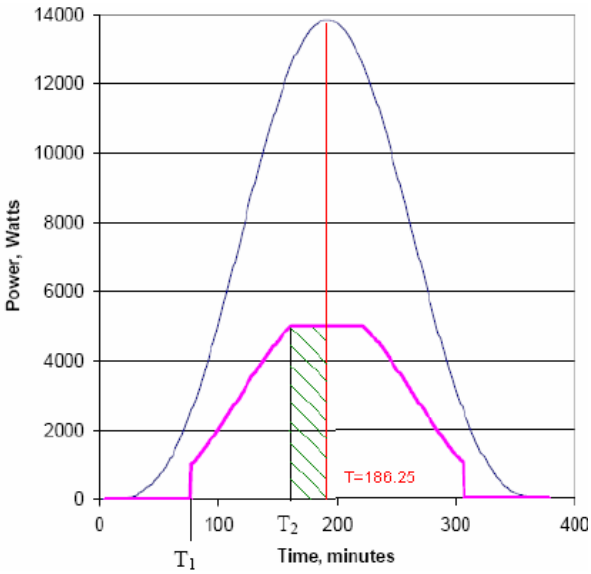

Figure 5. Power output over a half-cycle.

So, the energy harnessed during one quarter of the cycle would be given by:

$$\int P dt = \int_{T_1}^{T_2} C_p \frac{1}{2} \rho A V_{max}{}^3 \sin^3 \omega t + P_{rated} [186.25 - T_2]$$

1.4. TECHNOLOGY REVIEW

1.4.1. Types of turbines

Marine current turbines are classified depending on the way they interact with water in terms of motion. A rough classification would then make a difference between rotational and oscillating devices.

These devices can in turn be classified in terms of the direction of their movement, considering either vertical or horizontal turbines. In case of the rotational devices this refers to whether they are fixed with either a horizontal or a vertical axis, and in the other case it refers to the oscillation itself.

So, the whole of the different models available could be classified as follows:

- Rotational machines
  - Horizontal axis
  - Vertical axis
- Oscillating machines
  - Horizontal axis
  - Vertical axis

Both the horizontal and vertical axis rotational machine can be subdivided regarding how they interact with the flow, and so we can consider shrouded turbines [13], when the flow is deflected by some surrounding structure before entering the turbine, and free stream turbines, when the flow enters the turbine without any prior deviation.

That deflection of the water is meant to concentrate the velocity of the flow allowing the turbine to have a smaller diameter and a higher rotational speed however, the Betz's law is still in force regarding the frontal area of the turbine, and the speed is also limited because of cavitation issues. This type of turbines is meant to be arranged in very compact groups perpendicular to the direction of the flow, making up the so-called tidal fences [14].
Other classifications can be done regarding the type of fixing - either supporting structure or mooring system - , or the secondary energy conversion system.
This piece of work will anyway focus on rotational machines and more specifically on the horizontal axis ones working with a free stream.

- Free stream horizontal axis turbines:

The horizontal axis marine current turbine could be considered as the "aquatic sister" of the standard wind turbine.
The blades are joined to the hub of the rotor and they show a general greater thickness all along the aerofoil section than a wind turbine, due to the higher water produced loads. These blades are generally pitch variable, so the angle of attack of the flow can be changed in order to optimize the performance of the turbine ensuring maximum efficiency for the range of flow speeds given in the site, and also to avoid exceeding the rated power of the motor. Another important application of this blade pitching is to allow the turbine to operate in bidirectional tidal flows, setting the proper angle for either the up or the downflow.

The principle of operation is very simple, the flow enters the device perpendicular to the plane of the rotor, the resultant hydrodynamic forces from the flow covering the hydrofoil section of the blades act in the plane on the rotor generating a torque which is transferred through the shaft.

A model of these turbines is shown in figure 6 below:

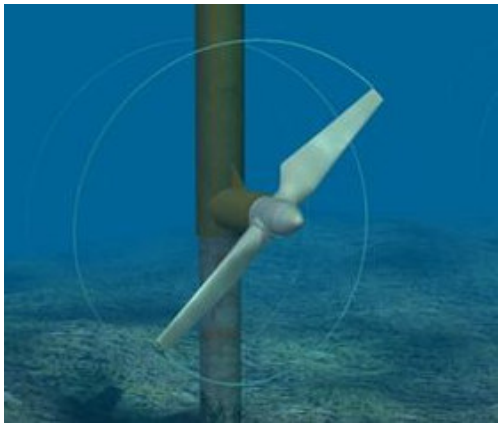

Figure 6. Horizontal axis marine current turbine (Source: www.esru.strath.ac.uk)

1.5. INSTALLATION

The most successful prototypes of horizontal marine current turbines so far have been installed on a tubular steel pile which carries the forces produced by the weight of the components, the operation of the rotor and the environmental loads.

The foundation of the pile is achieved by introducing it into a steel line which lines the socket, with a spigot inserted below it [15].

The nacelle to which the rotor itself is engaged is attached to the pile by a steel collar, which can be actually lifted over the water surface by a hydraulic ram. The function of this is allowing the testing and maintenance of the turbine.
All these elements are shown in the schematic below:

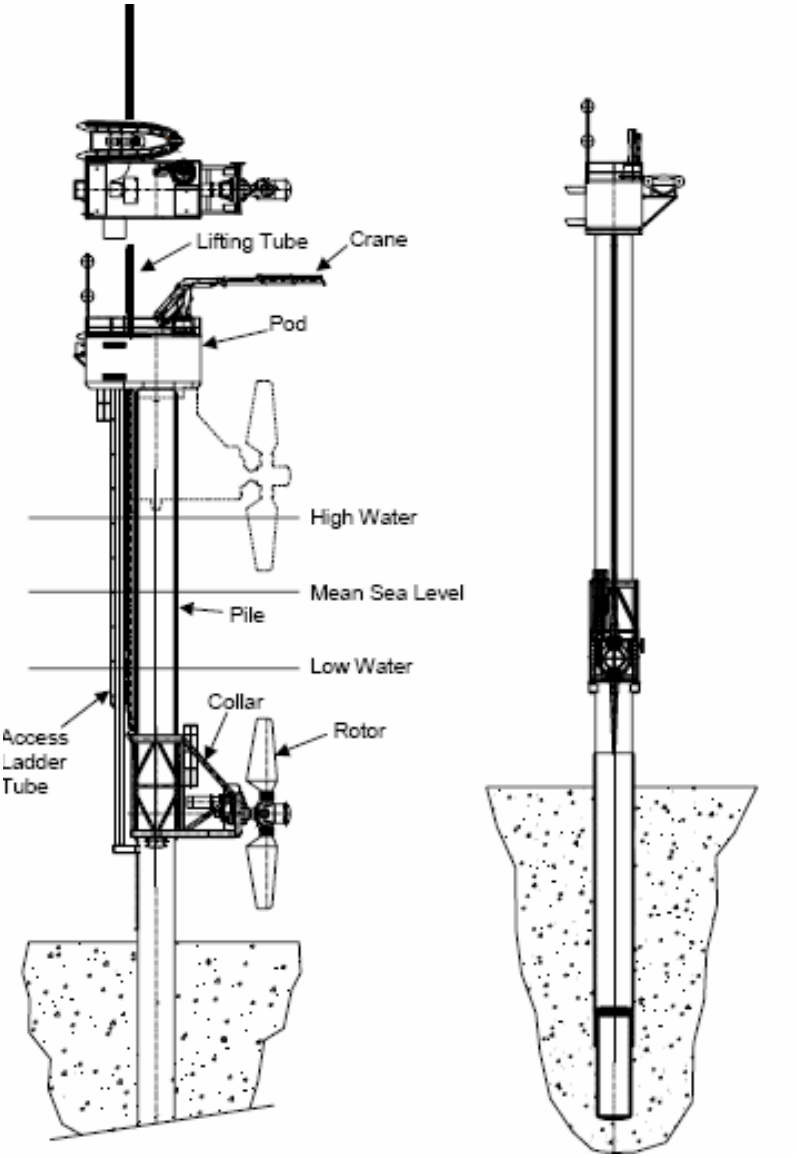

Figure 7. Marine current turbine arrangement. [15]

The nacelle of the turbine contains the mechanism to control the pitch angle of the blades, a large ratio gearbox to couple the shaft of the turbine with the generator, and the generator. The energy produced by the last is transported to the proper substation by a submarine DC cable.

A more detailed view of the nacelle is shown in figure 8 below:

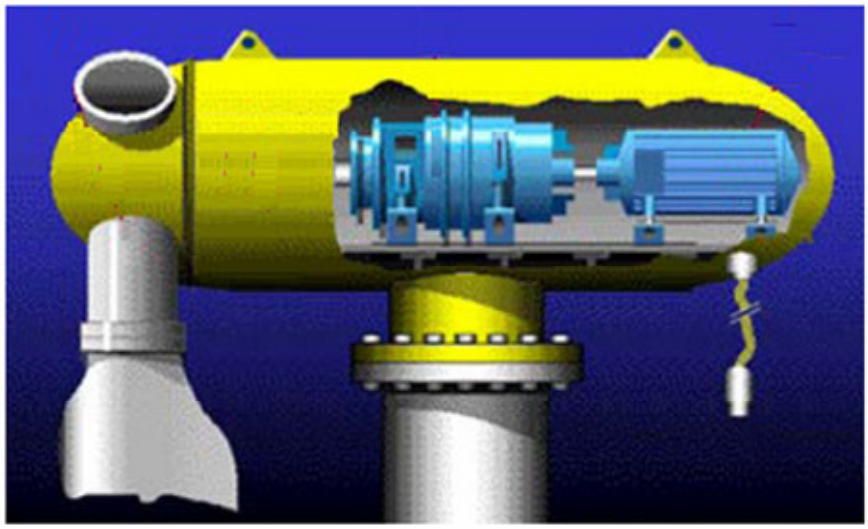

Figure 8. Inside view of marine current turbine nacelle.(Source: tidevannsenergi.com)

1.6. DEVELOPMENT

Over the last few years tidal energy development have gone through a boost, with many prototypes being tested in real coastal sites. The testing of these prototypes is a key issue in order to understand and improve how these devices work in realistic operational conditions, as well as to accurately find out which level of maintenance are required, monitor the performance and many other asks only achievable by experimental simulations. This stage has also a major importance as it is the previous step to start arranging and testing tidal farms.

SeaFlow and SeaGen – both developed by Marine Current Turbines Ltd. – have been the two most renowned and successful projects so far.

1.6.1. SeaFlow

SeaFlow was installed on the North Devon coast, England, in the summer 2003. It consisted on a horizontal axis marine current turbine, with a rotor of 12 m giving a rated power of 300kW in a current of 2.7 m/s, with a hydrodynamic conversion efficiency greater than 40% [15].

The whole system was mounted on a 2 m diameter monopole, and the whole installation process was carried out from a jack-up platform. The turbine can be raised over the water surface for maintenance, monitoring systems were installed, and a mathematical model for optimising the model in terms of size, capacity and cost was developed.

The appearance of the model is shown in figure 9 below:

Figure 9. The SeaFlow turbine.

1.6.2. SeaGen

SeaGen was installed in Strangford Lough, Northern Ireland in April 2008. With a twin rotor giving an output of 1.2 MW [, SeaGen is the logical evolution of SeaFlow. Mainly with in identical technology, the inclusion of two rotors increases the power output without a significant change on the overall installation process, and hence making the cost of the whole commissioning more profitable. The rotor of SeaGen, waiting for installation, is shown in figure 10 below:

Figure 10. SeaGen twin rotor.

However, what makes a difference in SeaGen is its commercial character. SeaGen has been the first ever grid-connected marine current turbine prototype, making this technology more real on July 2008.

The next step of the project would then be the installation and testing of a pre-production array of turbines.

The whole appearance of SeaGen is shown in figure 11 below:

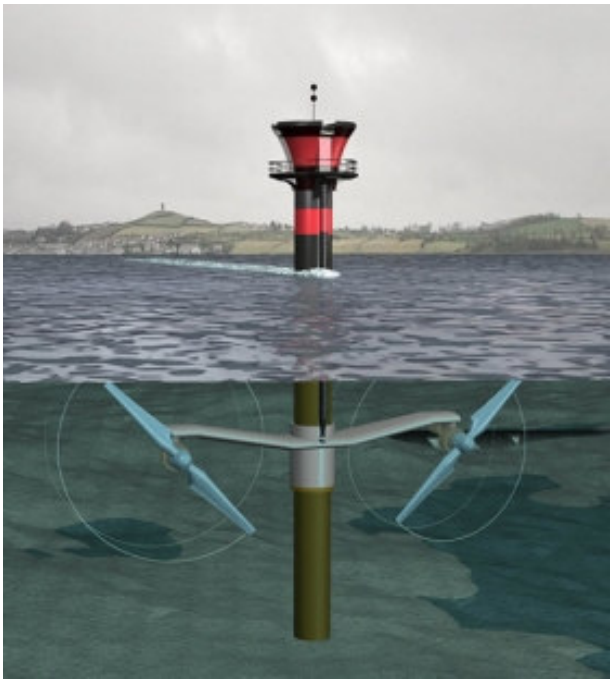

Figure 11. The SeaGen project.

1.6.3. Grid connections

As for the integration of marine current turbines into the electricity supply network, one of the main advantages of this technology is the fact that, although tidal cycles are quite complex, they are subject to a predictable schedule, so the power output can be managed and supplied easier and safer than with other renewable energies, where more variability is involved.

This is key factor regarding the future development of tidal energy, as there is the possibility of scheduling the power output and even matching it with local energy demand variation in case some energy storage systems were installed. This would enhance grid stability and contribute to the technical exploitation of marine current turbine farms, boosting their economical viability.

However, there is a big issue affecting the wide spread exploitation of this technology: the lack of grid connection points close to the tidal farms locations.

The available connections are likely to be to distribution networks serving small local coastal populations, whom capacity is very limited to take in projects of tens of megawatts if reinforcement modifications are not carried out [16].

The main constraints regarding grid connection and distribution are shown in figure 12 below:

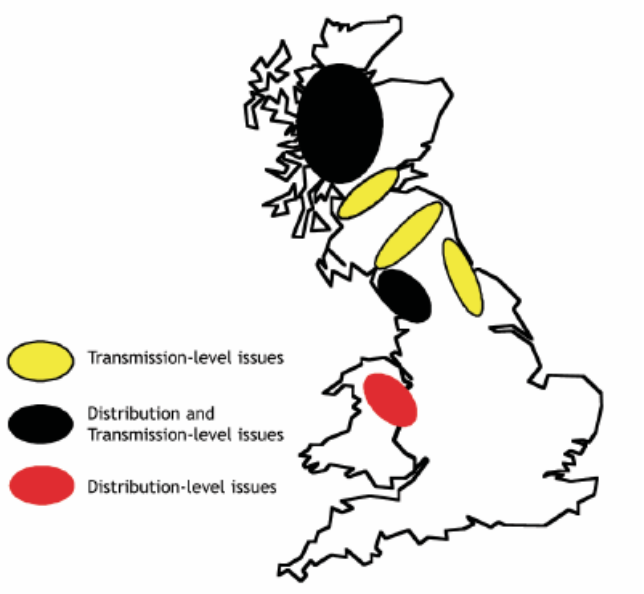

Figure 12. Main system capacity constraints [16]

These issues affect also other renewable energies, such as wind and wave power, however, tidal energy is the most harm as the available are more limited and very specifically located. In addition to this, and as capacity is already too short to accommodate proposed wind farms, marine turbine projects might be put aside due to their higher initial risk and cost.

1.6.4. Cost of energy

The cost of a type of energy is a useful way to analyze its technical situation and level of widespread exploitation, and compare them with those from its competitor energies.

The cost of tidal energy is basically depending on capital costs, operation and maintenance costs and the amount of electricity produced. And as in every technology, the device itself will be economically viable as long as the income produced by the saleable energy is greater than the cost of producing it.

The capital cost of a marine current turbine can be mainly breakdown into mechanical and electrical (including the whole design and manufacturing process of the rotor and the devices required to output and arrange the mechanical energy into electricity), structural (including the supporting structure as well as its foundation and off shore conditioning) and grid connection (including sub sea cables and switchgears). The individual contribution to the overall capital cost of these and some others is shown in figure 13 below or a typical tidal stream farm:

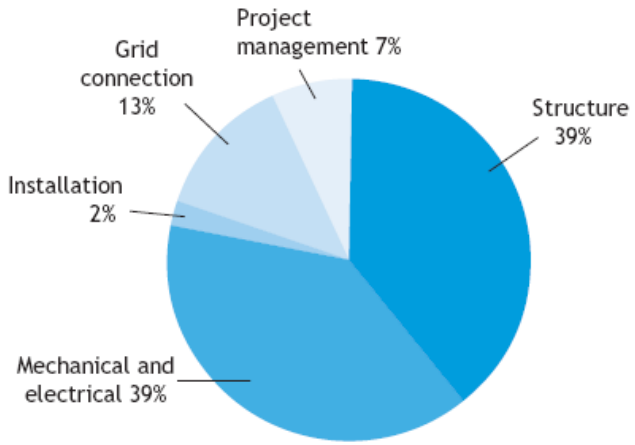

Figure 13. Breakdown of capital costs for a tidal stream farm.[16]

The operation and maintenance cost refers mainly to the cost of both scheduled and scheduled overhauls, components replacement and monitoring of the device performance.

These costs, as well as the capital ones, are highly specific for each site, and they are subject to significant variations in their individual contribution to the overall cost depending basically on the size and location of the tidal farm.

According to this cost, and considering present values for operational and maintenance cost and energy production, the cost of energy can be obtained as show below:

$$\text{Cost of energy} = \frac{\text{Capital cost + Oper. and Maint. Cost}}{\text{Energy Production}}$$

This way, cost from tidal farms in a first stage has been predicted between 9 p/kWh and 18 p/kWh, with central values between 12 and 15 p/kWh [12].

However, and in the same it happened with wind energy, there is big margin of reduction as the installed capacity increases, bringing about improvements in technology and more efficient exploitation patterns.

Estimations suggest the cost of energy would have drop to 7p/kWh by the time 1GW capacity has been installed, as shown in figure 14 below:

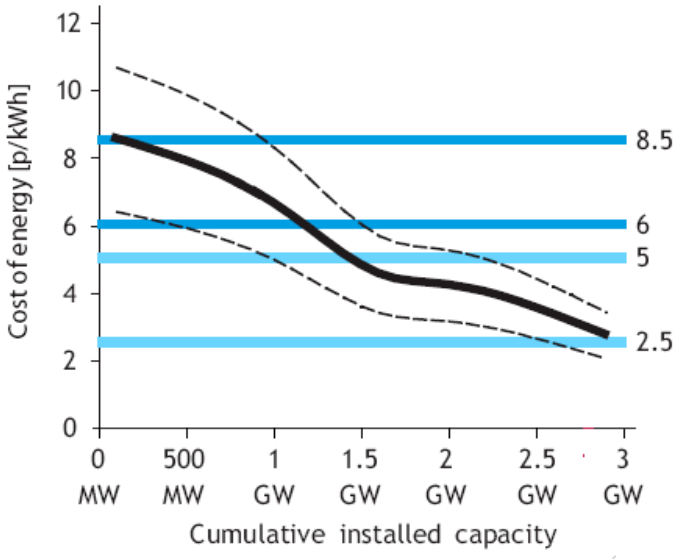

Figure 14. UK Tidal stream cost-resource curve.[16]

1.7. ENVIRONMENTAL IMPACT

The environmental impact tidal power might produce is not entirely known yet, as not real full scale tidal farms have been installed so far. However, the impact is projected to be very small.

Main aspects considered are the impact of the energy extraction on the bathymetry of the site, as well as on the local wildlife.

Some studies [12] suggest the energy extracted by the marine turbines would actually reduce the average speeds on the site, and hence reduce the energy available, as well as alter the lay out of the channel due to a reduction in the sediment transportation within. However, this issue would be highly dependant on the characteristics of each specific site and on the energy harnessing pattern of a hypothetic tidal farm. These aspects will be further analyzed in the section Basis of the project.

Regarding wild life, the rotor of a marine current turbine rotates at quite a slow speed, avoiding the possibility of local fauna colliding with the devices.

The visual impact would not be significant either, a tidal turbines would be almost totally immersed, avoiding locals to be perturbed, and with the proper signalling to avoid an unlikely shipping crash. A view from the shore of the turbine installed for the SeaFlow project is shown in figure 15 below

Figure 16. View if the SeaFlow project from the Devon coast.

The total potential impacts of this technology are shown in table 2 below:

	Scale				Duration			Residuals		Significance		
	Local	Regional	National	International	Short term	Medium term	Long term	No residuals	Residuals	Major	Moderate	Minor
Physical environment												
Wave climate	✓					✓		✓				✓
Flow	✓					✓		✓				✓
Sea bed / sediments	✓					✓		✓				✓
Water quality	✓				✓			✓				✓
Biological environment												
Habitats/benthos	✓					✓		✓				✓
Marine species	✓					✓		✓				✓
Birds	✓					✓		✓				✓
Landscape												
>3km	✓					✓		✓				✓
2-3km	✓					✓		✓				✓
1.5-2km	✓					✓		✓			✓	
1-1.5km	✓					✓		✓		✓		
Fisheries	✓					✓		✓				✓
Navigation	✓					✓		✓				✓
Noise	✓					✓		✓				✓

Table 2. Summary of potential environmental impacts [15].

2. DESCRIPTION OF THE PROJECT

2.1. REASON

Over the last few years, many studies have focused on the numerical fluid modelling of marine current turbines as a way to understand how this technology works.
These studies have mainly focused in three different aspects:

The characterization and analysis of the wake produced by the turbine, trying to work out its shape, magnitude, propagation patterns, and how it is affected by the boundary surfaces and the performance of the device itself.

The analysis of the array effects when marine current turbines are arranged in farms, basically focus on searching for the most advisable lateral and longitudinal spacing between the devices and for the optimization of the overall power output.

The study of how the installation and exploitation of marine current turbine farms can affect the natural conditions of a site regarding average flow speeds, among other environmental impacts.

However, and after a lot of progress done, there is still a huge uncertainty regarding most of the issues mentioned above. Because of this, and springing from the lack of experimental simulations in this field, this piece of work tries to break the ice and step into the analysis of marine current turbines through real physical models, as a way to shed some light on the issue by the always challenging and revealing empirical simulation.

2.2. METHODOLOGY

Three very small scale models of marine current turbine were designed, manufactured, tested and maintained in order to reproduce as far as possible the way this technology works.

A small scale array was arranged with these models and tested inside a flume.
This array was tested for different configurations of the turbines both regarding location and electrical loading ratio within the array.

Measurements of flow speed, voltage, current and power output were taken and recorded during the tests.
Those measurements were analyzed and the results were shown together with the conclusions drawn.

2.3. OBJECTIVES

- Analyze the array effects in a small farm of marine current turbines, with special focus on the wake and the blockage effect produced by rotating devices.

- Show how array effects affect the energy production of the turbines depending on their location within the array.

- Study how the variation of the electrical torque met by the turbines when generating a power output might either magnify or reduce the array effects.

3. BASIS OF THE PROJECT

3.1. ARRAY EFFECTS

Marine current turbines are likely to be installed in most sites available for tidal energy harnessing according to an array configuration. It is this way that the overall energy production can be cost-effective and therefore suitable for a grid connection.
This array layout will make it essential for both designers and producers to be aware of the array effects driven by this configuration, as it obvious each device will have an impact on the performance of the devices surrounding it.

According to this we can define an array efficiency [6], which will indicate how each turbine performs within the array. This value will be obviously different for each turbine and is given by the following expression:

$$\text{Array efficiency (\%)} = \frac{E_{\text{farm turbine}}}{E_{\text{free turbine}}} \cdot 100$$

With:
$E_{\text{farm turbine}}$: machine output in the farm
$E_{\text{free trubine}}$: machine output without the influence of other machines

The main effects to be considered regarding the array efficiency for each device and therefore the overall energy performance of the array are the blockage effect and the wake effect.

3.1.1. Blockage Effect

The presence of the rotors can cause a blockage effect [3] to the flow. This effect is due to the resistance the rotors present against the flow, which may divert it from their swept area in the search for an easier way to pass through.

Blockage effect is often characterized by the blockage ratio [3], a dimensionless factor which defines the density of rotors in the cross-sectional area of the channel.
The value is given by the following expression:

$$\text{Blockage Ratio} = \frac{A_{\text{occupied}}}{A_{\text{occupied}} + A_{\text{free}}} \cdot 100$$

Where A_{occupied} is the overall swept area of the rotors and A_{free} is the cross-sectional area of the channel free of rotors, as shown in figure 17 below for a row of three rotors in an ideal channel.

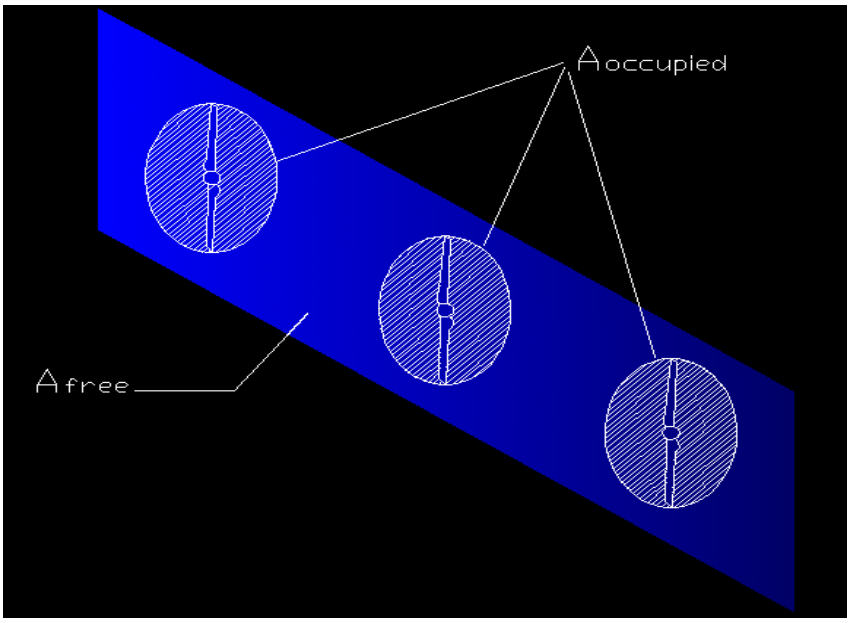

Figure 17.Hypothetical cross-sectional area of a row of MCTs.

Blockage can be considered to be either harmful or useful when analysing array performance depending on the rotor layout, and especially on the lateral spacing.

In the first case, and assuming there were many rotors in the same row so a blockage effect was caused, the flow may be diverted from the area occupied by rotors, constraining and hence accelerating it between the array and the boundary surfaces which surround it. This would directly affect the performance of the array, and might decrease its energy production.

Blockage effect has already been observed when analysing the performance of marine current turbines through numerical simulations. Figure 18 below was obtained from a 2D CFD simulation of an array of 5 marine current turbines [8].

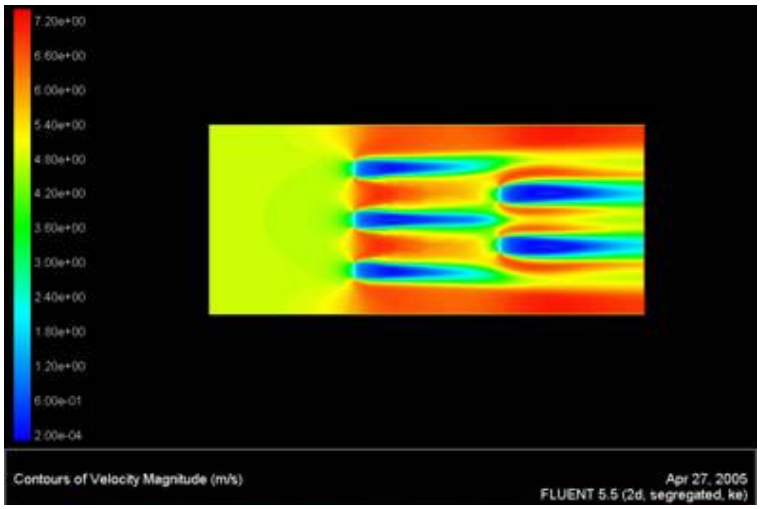

Figure 18.Velocity contour (m/s) through a 5 MCTs array.

Flow being accelerated due to blockage effect can be clearly seen especially in the gaps between the array and the lateral boundary walls, where flow speeds are 31% higher than in the upstream flow.

These findings match with those from other empirical studies, where flow speeds higher than the inflow speed were found [7] around the sides of a rotor at model scale, again due to blockage effect.

In this situation and according to some authors, enough lateral spacing between the rotors would be crucial in order to allow a sufficient quantity of free flow to pass through lessening the blockage effect.

Blockage effect is obviously highly dependent on the dimensions of the channel and the number of rotors acting against the flow, therefore, it is important to consider, when working at small scales, whether a given distribution of rotors would block the flow too much in comparison with the blockage the same distribution would actually produce in a real site at a real scale, where the boundaries will be further away from the array area. This problem occurs with wind turbines, which suffer from blockage effects in the wind tunnel tests while no blockage effect is ever going to happen in a real wind farm. In such situation a blockage effect correction should be considered.

In case there is blockage effect, but not enough space for the flow to be diverted - due to a high density of rotors for example -, the flow would have no option but to pass through them, with the consequent energy extraction.

It is known that the maximum energy extractable by a device in an unbounded flow is given by the Betz's Law, fixing a maximum Cp of 16/27. However, higher power productions per rotor area can be reached when employing blockage effects.
2D theoretical model studies have obtained increases in Cp by 18.7% at induction factors of 1/3 (corresponding to the Betz limit) as blockage increases [9].
This different configuration, in which blockage effect would be enhanced instead of lessened, would require a large amount of rotors in the same row and, according to the momentum conservation theory, flow speed would be dramatically reduced downstream of such a row due to the high energy extraction carried out .

3.1.2. Wake effect

The movement of the rotor harnessing the energy of the flow creates a wake whose speed is lower than that of the upstream flow due to the energy which was extracted from it.
The wake is characterized [5] in two different zones: the near wake and the far wake.

In the near wake, vortices from the blade tips and the support structure bound the slower flow from the free-stream flow avoiding fluid mixing. This near wake lasts from 0-3/4 rotor diameters [5], until the turbulence from the free-stream flow destroys the vortices and the fluids begin to mix.

The far wake, turbulence mixing has already broken down the wake and increases its velocity until a value close to the value of the flow velocity upstream of the rotor is reached.
The free-stream velocity would then be a key factor regarding the velocity of the wake and the distance it persists far downstream of the turbine.
A key factor of the wake regarding its influence on the array performance is its expansion. As an amount of energy has been extracted from the flow, it moves slower than the free stream flow, and hence expands to conserve momentum. This expansion makes the wake wider both in width and height [5], so it can certainly reach and affect

both the water free surface and the devices downstream if it is not recovered in time by the free stream flow.

There are other factors affecting the wake of a marine current turbine:
The performance of the device is one of them [5], consequently, the more energy is extracted from the flow by the device the lower the initial velocity of the wake.

Turbulence, generated either by the ambient conditions or by the device, is another key feature affecting the wake [5]; ambient turbulence might be generated both close to the sea bed and to the water surface, due to the shape and the elements of the bed in the first case and to the waves and the swell in the second. Device turbulence will be generated mainly by the blades and the support structure and it will not last further than the near wake.
The presence of boundary surfaces themselves, both above and below the device also affects the wake of marine current turbines [5]. These surfaces limit the movement of the flow vertically, forcing a greater lateral movement.
Enough downstream spacing between the rows is now essential to allow the wake to sufficiently mix with the free flow, allowing the flow speed to recover and hence curbing the wake-induced energy losses of the devices downstream.

The main and final consequence of the wake effect is that there will be a flow decay downstream of the rotors, where the energy has been taken from the flow and converted into useful work. Therefore, the downstream flow will have a lower speed; this will directly affect the energy performance of any device downstream and will be the main reason for the need to consider a downstream spacing between the devices.

Studies from Myers and Bahaj [3] estimate the flow decay by applying a momentum conservation theory, so the reduction in the momentum of the flow through a row of marine current turbines will define the new flow speed to a new row of turbines situated downstream.
The relationship between the inflow velocity and that just downstream of the rotor is given by the following expression [3]:

$$U_W = (1 - 2a)U_O$$

With U_W = wake velocity, U_O = inflow velocity, a = rotor axial induction factor

The optimum value of *a* is equal to 1/3 and is reached when the rotor is operating at maximum efficiency [4]. The higher the rotor axial induction factor, the higher the velocity deficit downstream.

The new downstream flow speed would be then defined as follows [3]:

$$U_{DR} = \left[\frac{A_{array}}{A_T}(1-2a) + \frac{A_{free}}{A_T} \right] \cdot U_O = R_{DF} \cdot U_O$$

With:
A_{array} = cross-sectional area occupied by rotors.
A_{free} = cross-sectional area free of rotors.
A_T = total cross-sectional area of the array.

The term in brackets was defined by the authors as a dimensionless row velocity decay factor (R_{DF}).

3.2. ARRAY CONFIGURATIONS

There are different theories regarding the most appropriate layout for an array of marine current turbines.
Although clear uncertainties are found in this area, especially regarding the influence each device will have on the devices downstream due to blockage and wake effects, and there is an obvious lack of experimental tests in real sites, the main arguments refer to whether the bulk energy production should be achieved in a hypothetic first row of the array -like the concept of a “tidal fence”- with a high density of big rotors (i.e. a high blockage ratio) or on the other hand go for a more distributed energy production with a longer array built up of smaller devices.

These configurations bring about different performances in terms of potential environmental impact, efficiency of the devices, energy production and of course cost-effective considerations.
It is important to mention that these two possibilities fit into the so-called “Farm Method” [12]: an extraction methodology according to which the number of devices and therefore the extracted energy is only dependent on the size of the device, its efficiency and the density of devices within the array area.
The differences between these two possibilities will be addressed below.

3.2.1. High density of rotors

The option of placing a number of big rotors and hence obtaining a high blockage ratio - assuming the flow is not diverted between the devices and the boundaries -, would bring a great flow decay downstream of the devices as a big percentage of the energy available in the flow would have been harnessed.

Coming back to a comparison with wind turbine technologies, this is pretty much the option chosen when installing arrays of wind turbines. Experience in the wind turbine industry has proven that large rotors in a relatively small spacing are far more efficient both technically and economically speaking. However, this can not be automatically accepted for marine current turbines, given the important differences in the characteristics of the environment in which each technology is applied.

Marine current turbines are placed in relatively narrow channels, and hence much more close to the boundaries than wind turbines so a number of big rotors acting against the flow would have a clear impact on the local characteristics of the site.

In this high density configuration, long distances would be required for the free stream to recover before more rows of marine current turbines could be installed. There is an obvious correlation between the amount of energy extracted at a point along the flow and the distance from that point for the flow to recover - the greater the energy extraction the lower the velocity of the flow just downstream of the device.
That distance may be affected by other parameters, such as the initial upstream velocity, the turbulence intensity or the morphology of the channel itself, however,

the correlation can be clearly seen in figure 19 below, obtained from numerical modelling for a mid depth layer of an ideal channel as a consequence of artificial energy extraction [10]:

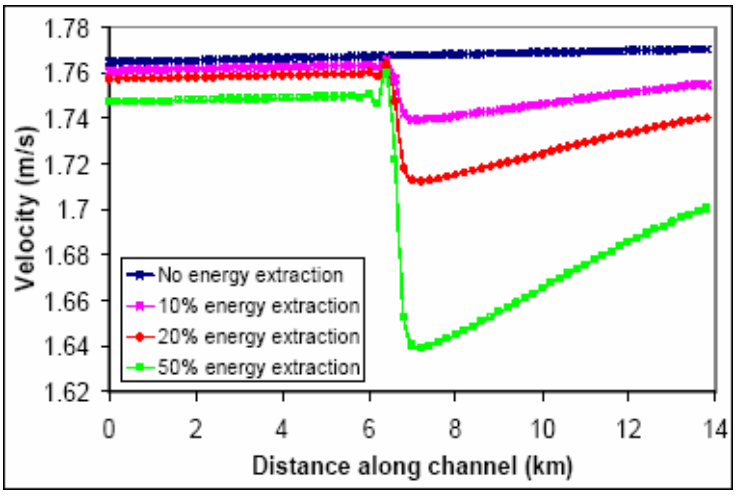

Figure 19. Velocity profiles for different energy extraction rates

Another important effect of the exploitation of a site with a high density of large rotors would be the intensification of the changes in the water depth. As it was previously mentioned in section 3.3, the presence of a free surface allows the water depth to change, therefore, the extraction of a big amount of energy carried out at the same point by that group of large devices might bring about a big change in the water surface. This change would not only affect the performance of any device placed downstream but also the physical characteristics of the channel itself.

Work from the Robert Gordon University, analyzing the effects of different percentages of raw kinetic energy extraction for a theoretical Pentland Firth type site showed the variation of surface elevation in the channel, the results are shown for a 65m depth, 2 m/s unexploited depth-averaged flow speed in figure 20 below:

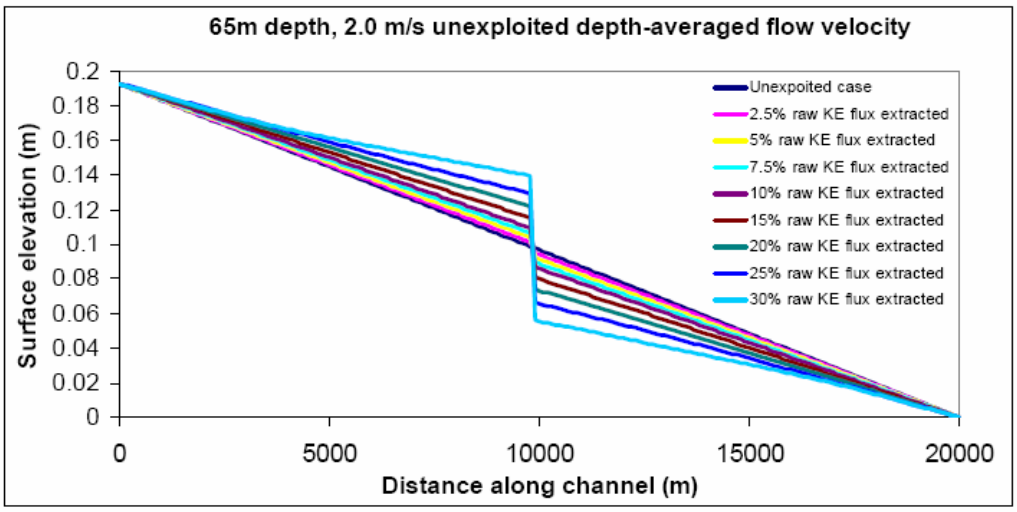

Figure 20.Elevation across the channel for different energy extractions [12]

It is clearly seen how a larger proportion of the total channel's head drop takes place at the energy extraction point rather than along the channel.

Apparently, this high density configuration might imply a more significant environmental impact on the site. Apart from the obvious reduction in the energy available in the flow, the reduction of the flow speed would also affect the transport of sediments, among other environmental aspects.

Some work developed in [1], showed the effects of energy extraction with an array of marine current turbines in terms of reduced average speeds. An array of 160 units, with a rated speed of 2.5 m/s, axial spacing of 15 rotor diameters and lateral spacing of 4 rotor diameters, taking up an area of roughly 2 km^2, was simulated through CFD modelling. A distribution of cubed speed was spatially averaged over the area of energy extraction (the area of the array) for two different situations: with energy extraction and without energy extraction. The histogram obtained is shown in figure 21 below:

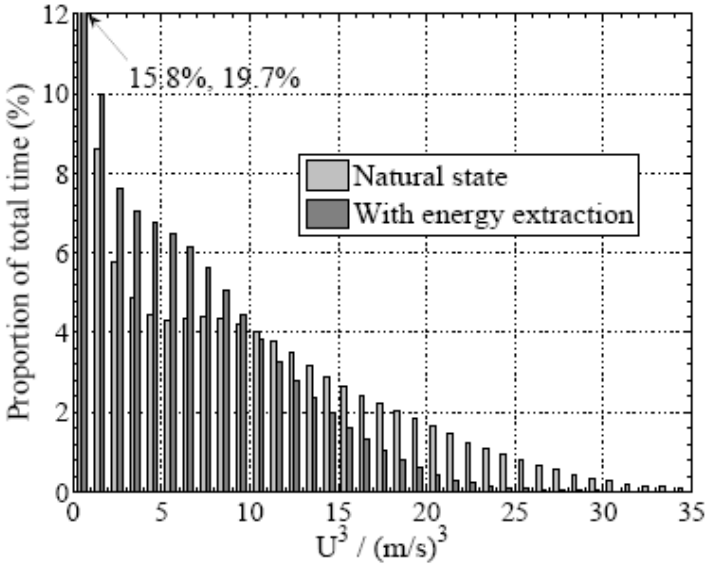

Figure 21.Histogram of cubed speeds averaged over the array area [1]

As it can be seen, some increases in speed were found, presumably due to the flow being accelerated because of blockage effect, as well as a significant reduction in the rated speed of the array, 15 $(m/s)^3$. This reduction – of about one third -, would mean a reduction of one third in the available energy at that rated speed.

The averaged speed is obtained from the different speeds found in the array area, and the lower ones would be found in the last rows of the array, as a consequence of the flow decay caused by the devices upstream. According to this, the effects of the flow speed reduction would be gradually increasing as we move towards the end of the array. This should certainly be considered when designing the devices – especially in terms of size and rated speed – in order to obtain an optimum performance according to the place they occupy within the array.

3.2.2. Low density of rotors

The installation of smaller devices with a higher spacing - therefore causing a lower blockage effect -, would result in an array made up of a higher number of rows and hence in a more distributed energy production.

The lower percentage of energy harnessed per row – in comparison with the high density configuration -, would imply lower flow decay downstream of each row of devices, defining a different array performance and configuration.

An array with this low density configuration and the same rated power as a high density array – like the one previously described -, might have a longer distance, as less and smaller devices would be fitted in each row. However, and as the longitudinal spacing between rows would be significantly shorter - due to the higher flow speeds downstream of each row – there could be a balance between the higher number of rows and the shorter spacing leading to a shorter overall array distance.

The advantage of this configuration would be the lessening of the effects previously addressed regarding the physical characteristics of the channel.
A lower density of rotors per row would reduce the possible changes in the water depth, as less energy per row would be taken from the flow. In the same way, the reduction in the flow speed would not be that dramatic, as lower speed deficits would appear and flow would be allowed to recover more frequently, lessening potential environmental effects.

3.2.3. The case of Alderney Race

Some work developed by Myers and Bahaj [3] simulated the electrical power potential harnessed by an array of marine current turbines.
This array was actually made up of different sub arrays, whose turbines had different rotor diameters, as shown in figure 22 below:

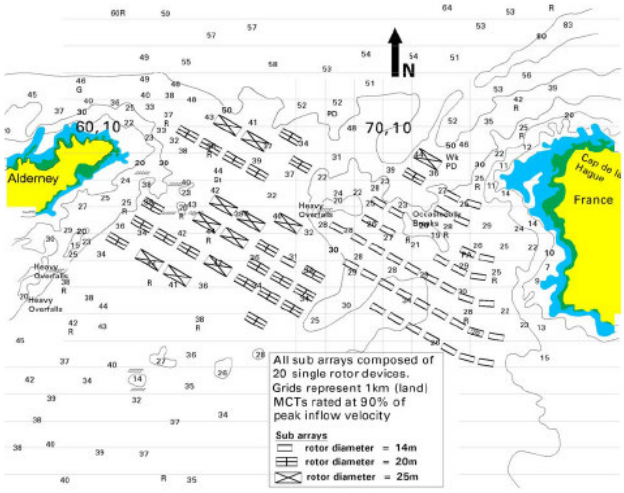

Figure 22.Race of Alderney array layout [3].

This configuration would be a possibility to make the most of the reduced average flow speed downstream of the first rows of devices. However, the fact that flow goes in two directions and the need for optimizing the array according to that would be serious obstacles to overcome.

3.2.4. Significant Impact Factor [SIF]

There is another extraction prediction methodology – "The Flux Method" [12] – based on the use of only the incoming kinetic energy flux across the front cross-sectional area of the flow channel, and independent of the device type, efficiency and density.

Assessment of the UK Tidal Stream Resource made by Black & Veatch showed the need for constraining the Farm Method, as it was predicting an over-extraction due to improvements in the efficiency if the devices and a better understanding of the spacing required by the devices. This constraint is represented by the Significant Impact Factor [SIF] [12].

Some authors have used this factor when analyzing the exploitation of marine current turbine sites and their environmental impact. According to their theories, only a limited percentage of the total energy available in a site can be harnessed without significantly affecting the characteristics of the site, especially in terms of flow speed.

The Significant Impact Factor indicates then the maximum percentage of energy which could be extracted from a site without causing a significant change in the general flow speed, and hence avoiding potential both environmental and economical impacts due to the reduction in the available energy of the site.

The values considered for the Significant Impact Factor range from around 10% to 50% [11] of the total kinetic energy in the site, however, these values are simple assumptions based on numerical simulations which need obviously to be validated with experimental data.

In addition to this, and assuming these factors are right, they would be highly dependant on the characteristics of each site. In channels where the flow is generated by a head difference at one of the ends of the channel and the flow can not affect the

elevation of the bodies of water, the SIF would have low values. On the other hand, higher SIF values could be found in stronger sites, where they are more free for the elevation boundary conditions to change.

Some illustrative values for the Significant Impact factor for different UK sites, together with the potential reduction of the flow velocity they might cause in the site are shown in table 3 below:

Site Name	Mid-range Velocity Change (%)	Acceptable SIF (%)
Pentland Skerries	15	20
Stroma, P. Firth	15	20
Duncansby Head, P. Firth	15	20
Casquets, Channel Islands	10	8
S. Ronaldsay, P. Firth	15	20
Hoy, P. Firth	15	20
Race of Alderney, Ch. Is.	10	12
S. Ronaldsay, P.Skerries	15	20
Rathlin Island	10	8
Mull of Galloway	10	12

Table 3.UK sites and SIF parameters [12]

3.2.5. Cost effective considerations

Setting the differences between the Farm Method and the Flux Method aside, there is a cost effective analysis which can be certainly applied to both extraction methodology. If we start to install an infinite number of marine current turbines was to be installed in a site, we would find out a certain point that the installation of more devices would no longer contribute to the overall energy produced by that array, in fact, that overall energy would be reduced if more devices were installed from that point.

Work from Agbeko, Love and Fitzpatrick [8] showed this tendency by simulating the power produced by an increasing group of turbines in a site at Pentland Firth. The results are shown in figure 23 below:

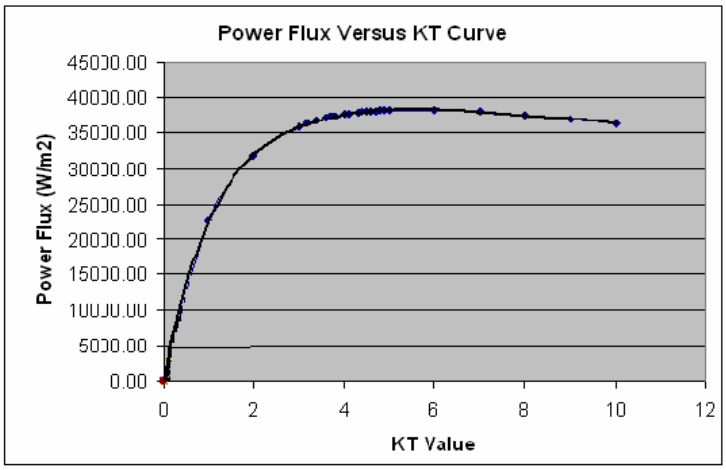

Figure 23.Power flux against number of turbines [8].

KT is a value representative of the number of turbines in the site. As can be seen, there is a number of turbines with which the maximum power per squared meter is obtained. However, the installation of turbines would have ceased to be profitable before that point. From the moment at which the gradient of the curve – power per turbine – starts to drop off at a certain rate is no longer profitable to include more turbines, as the increase in power would not compensate the cost of the turbine. This is something for the designers to seriously take into account when building an array of marine current turbines.

3.3. SIMILARITIES AND DIFFERENCES WITH WIND ENERGY

Although wind farms are also distributed in arrays and both technologies are quite similar, there are significant differences which have to be considered when analyzing the array configuration of marine current turbines, especially if knowledge obtained from either wind farm exploitation or wind turbine research is to be applied.

The main difference lies in the nature of the fluid each technology works with.
Marine current turbines work in underwater conditions, so the presence of two boundary layers must be considered: the sea bed and the water surface. The presence of this free surface at the top can make a substantial difference with wind turbine sites, where the whole atmosphere is involved, therefore there is effectively no upper boundary.
Marine current turbines extract energy from a tidal flow, and as the free surface enables the depth to change, that energy extraction may bring about a change in the depth of the channel. That change may be negligible for one single device, but quite significant if it is produced by a greater number of devices [5], like in the case of an array. The effects of this on the downstream flow conditions could seriously affect the performance of the devices downstream.
If the surface level were to drop, the cross-sectional area of the flow would be reduced, therefore, as the same volume of water is meant to pass through, the flow speed is accelerated. In the same way, that reduction in the cross-sectional area while the area occupied by rotors remains the same brings about an increase in the blockage ratio.

Regarding the location of the devices, flow speed is greater close to the surface, however, marine current turbines will have to work closer to the sea bed. This is not only due to the potential depth drops previously explained, but also because surface waves may disrupt the free surface affecting the higher layers of the water flow and increasing local turbulence.

All these factors will affect both the downstream and the lateral spacing within the array. The recovery time of the wake might be different for wind and marine technologies, and hence different downstream distances will have to be considered to allow the flow to get closer to its free stream velocity.
As for the lateral spacing, many tidal sites have purely bi-directional flows [5], and hence lateral spacing could be reduced in comparison with wind turbines arrays. This phenomenon has already been observed in real wind farm sites [6], where array losses were less sensitive to inter-machine distances when there was a clear predominant wind direction.

There have been several studies regarding wake recovery and array effects in wind farms, not only through modelling techniques but also through experimental data acquisition in real sites. Therefore, array performance of wind turbines is better known and uncertainties are less of a concern than with marine current turbines.

4. MODEL DEFINITION

4.1. THE FLUME

4.1.1. Location

The flume in which the measurements and tests included in this piece of work were taken is located in the Hydrodynamics Laboratory of the University of Strathclyde, Colville Building, Glasgow.
A view of this facility is shown in figure 24 below

Figure 24. University of Strathclyde flume.

4.1.2. Specifications

The flume has a length of 34.5 m and a width of 1 m.
The water is circulated along the flume by a pumping system with a maximum capacity of 140 l/sec, giving a maximum flow speed of 0.47 m/s.

This facility is quite old, and hence its water tank was brick made, increasing the number of sediments in the water and hence decreasing the underwater visibility, this was actually making difficult the taking of pictures while the devices were in operation.

4.2. ROTOR AND GENERATOR

4.2.1. Assumptions made

- Tip speed ratio

The tip speed ratio [TSR] shows the relation between the rotational speed of the tip of the blade and the velocity of the flow:

$$\text{TSR} = \frac{\text{tip speed of blade}}{\text{flow speed}}$$

A tip speed ratio of 4 was assumed for the calculations, a reasonable value for horizontal-axis turbines at maximum power. However, the real tip speed ratio obtained once the model was tested will be shown in section 4.5 below.

- Coefficient of performance

The coefficient of performance [C_p] indicates the percentage of energy extractable by a device in a flow from a theoretical maximum.

A coefficient of performance of 0.3 was assumed for the calculations. Meaning that only a 30% of the total energy available will be extracted by the device. A good turbine would give a coefficient of performance of 0.4 or even better, but the one we will be using is not, we are actually forced to use a rotor which does not have an ideal shape. The reasons for using this rotor are further explained in section 4.2.5.

4.2.2. Power

The power which could be extracted by one single turbine inside the channel is given by the following expression:

$$P = \frac{1}{2} C_p \rho A U^3$$

With:
C_p = coefficient of performance
ρ = water density
A = rotor area
U = flow speed

4.2.3. Rotor diameter

The rotor diameter was chosen according to the flow speed of the channel and for the turbine to power the DC motor properly.
It is obviously a critical factor that the rotor is able to meet the starting torque of the DC motor, or no generation will be ever achieved, and once the starting torque is met, is important for the motor to efficiently load the rotor, otherwise the motor will rev up and generation will not be satisfactorily produced.
Those are the two key factors for the rotor and the motor to work properly.

According to this, a wide range of rotor diameters was considered in order to match with the different options from the manufacturers in terms of speed and torque.
The rotor diameter will dictate the rotor speed and the torque at the rotor shaft, so these parameters were calculated as explained below:

The rotational speed of the rotor is obtained from the tip speed of the blades, which is given by the flow speed and the tip speed ratio, and the rotor diameter, as shown below for a rotor diameter of 12cm:

tip speed of blades = tip speed ratio (λ) · flow speed (U) = $4 \cdot 0.5$ m/s = 2 m/s

$$\omega_{rotor} = \frac{v_{rotor}}{R_{rotor}} = \frac{2 \text{ m/s}}{0.06\text{m}} = 33.3 \text{ rad/s}$$

$$33.3 \frac{\text{rad}}{\text{s}} \cdot \frac{60\text{s}}{1\text{min}} \cdot \frac{1 \text{ rev}}{2\pi \text{ rad}} = 318.3 \text{ rpm}$$

The torque at the rotor shaft is obtained from the expression of the power in terms of rotational speed and torque:

$$P = T \cdot \omega$$

The power of a single turbine with a 12cm rotor would then be given by:

$$P = \frac{1}{2} C_p \rho A U^3 = \frac{1}{2} 0.3 \cdot 998.2 \cdot \left(\frac{12}{200}\right)^2 \cdot 3.14 \cdot 0.5^3 = 0.21 \text{ W}$$

So the torque at the rotor shaft would be:

$$T = \frac{P}{\omega} = \frac{P}{33.3} = 6.35 \text{ mNm}$$

According to this process, different values of rotor speed, rotor power and torque at the rotor shaft were obtained for the different rotor diameters considered, as shown in table 4 below:

Rotor diameter [cm]	Rotor speed [rpm]	Rotor power [W]	Torque [mNm]	Torque [g.cm]
13	293,82	0,25	8,07	82,39
16	238,73	0,38	15,05	153,60
19	201,04	0,53	25,21	257,21
22	173,62	0,71	39,13	399,29
25	152,79	0,92	57,42	585,93

Table 4. Rotor speed, power and torque for the diameters considered

4.2.4. Generator

The manufacturer chosen for the motor was MFA, which offers a wide range of motors and multi ratio gearboxes which match with the characteristics required for this work.

The model chosen belongs to the 918D Series 25mm single ratio metal gearbox, which incorporates a three pole motor with sleeved bearings and a miniature gearbox of steel and brass construction with brass gears mounted on a 1mm thickness steel bracket.

The motor and gearbox dimensions are shown in figures 25 and 26 below:

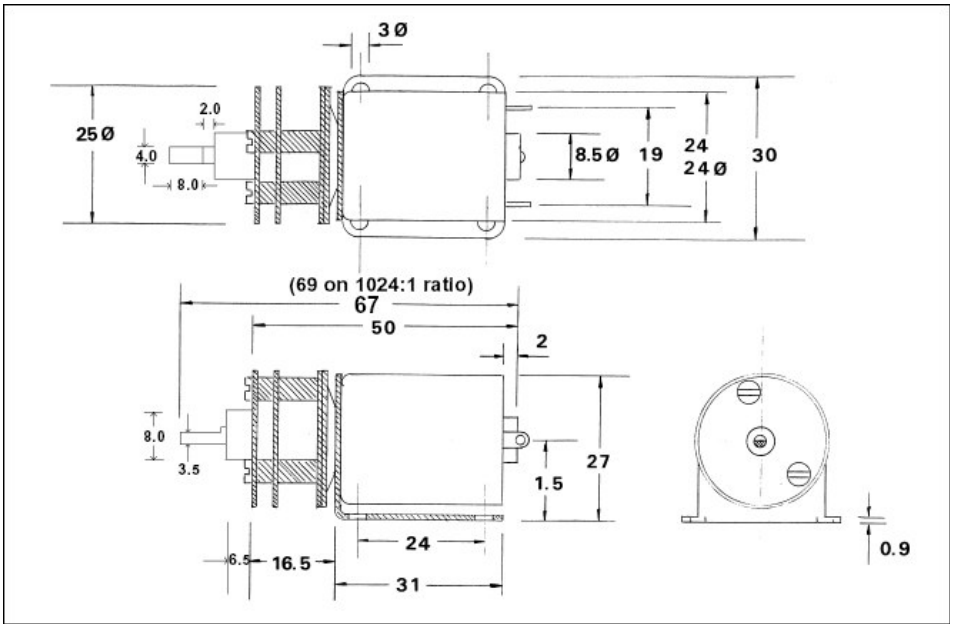

Figure 25. Motor and gearbox dimensions [mm].

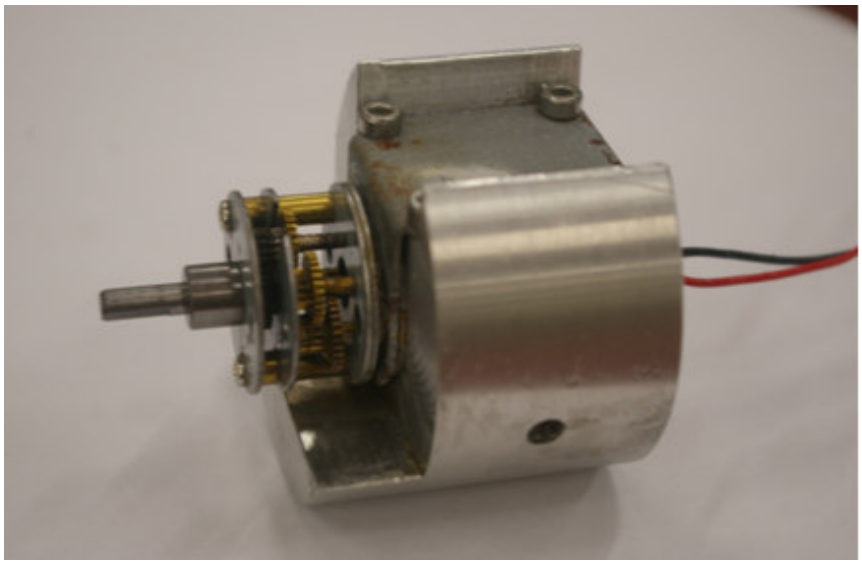

Figure 26. Mounted motor and gearbox.

The motor data are shown in table 5 below:

MODEL	VOLTAGE		NO LOAD		AT MAXIMUM EFFICIENCY						STALL TORQUE	
	OPERATING RANGE	NOMINAL	SPEED	CURRENT	SPEED	CURRENT	TORQUE		OUTPUT	EFF		
			R.P.M.	A	R.P.M.	A	oz - in	g - cm	W	%	oz - in	g - cm
RE - 280	1.5 - 3 .0	1.5v CONSTANT	4600	0.120	3750	0.53	0.160	11.53	0.44	56.2	0.86	62.0
RE - 280	1.5 - 3.0	3.0v CONSTANT	9200	0.155	7800	0.85	0.278	20.00	1.60	62.3	1.81	130.0
RE - 280/1	12 - 24	12v CONSTANT	8400	0.10	6300	0.30	0.347	25.0	1.62	44.87	1.389	100

Table 5. Motor data

For this application the motor will be used in reverse, i.e. working as a generator, therefore, those data are not very representative, in particular the efficiency, which could never be reached due to the characteristics of our application.

The main parameter to be concerned about is the starting torque the device will have when working as a generator; this will be the key value in order to choose the rotor diameter. Once the starting torque is met, a rotational speed in the interval from 150 to 300 rpm (as shown in table 5 above) would be reached (as long as the propeller used as a rotor has a TSR of 4).

According to this, a speed up ratio of 30:1 was chosen for the gearbox, so the generator will be working with a speed between 4500 and 9000 rpm in open circuit. That speed would define the voltage given by the generator.

4.2.5. Rotor selection

As there was a clear inability to manufacture a small scale rotor according to the dimensions and shapes employed in real marine current turbines, due to the lack of time and especially to the lack of the proper facilities for such a complicated task, it was decided to use an aero modelling propeller, shown in figure 27 below:

Figure 27. Aero modelling propeller

The aero modelling propeller will have to be used in reverse, for the curvature of the blades to be acting against the flow - just opposite to when it works as a propeller -. This will bring a drop in the efficiency of the rotor, as the leading edge will be now working as the traiching edge. However, this was the closest option to a real rotor, and that lack of efficiency should not be a problem as we are not looking for an efficient device.
All the devices included within the array will be manufactured in the same way, the array effects should then be satisfactorily analyzed, as all of the devices should perform almost identically.

In order to choose the proper rotor, different diameters were tried inside the flume. The first diameter which was actually able to meet the starting torque and rotate at an acceptable speed in open circuit was the 22 cm one. However, and in order to obtain a bigger margin of usage, taking into account that higher resisting torques will appear when the devices are working in a closed circuit, a diameter of 25 cm was chosen in order to provide higher torques at the rotor shaft.

4.3. ELECTRICAL SYSTEM

According to the characteristics of the project, there was the need of installing an electrical system in order to analyze the performance of the turbines in terms of power output.

As it was previously explained, the turbines within an array are affected by the devices surrounding them, and the drop in flow speed caused by the turbines upstream when harnessing the energy from the flow may affect the energy production of the downstream turbines.

4.3.1. Installation

Two wires were connected to the output terminals of the rotor so the power produced by the turbines could be accessible.

As the turbines within the array were going to be tested under different electrical loads, each motor was connected into a potentiometer, so different values of resistance could be selected in order to modify the resisting torque the turbines would have to meet.

In order to make a more practical layout for the system, the potentiometers were placed in a plastic board together with six connectors where some of the electrical measurements were taken.

In addition to this, a terminal block was connected between the set of potentiometers and the output from the motors in order to make electrical measurements easier.

The circuit diagram and the whole assembly of the electrical system are shown in figure 28 below:

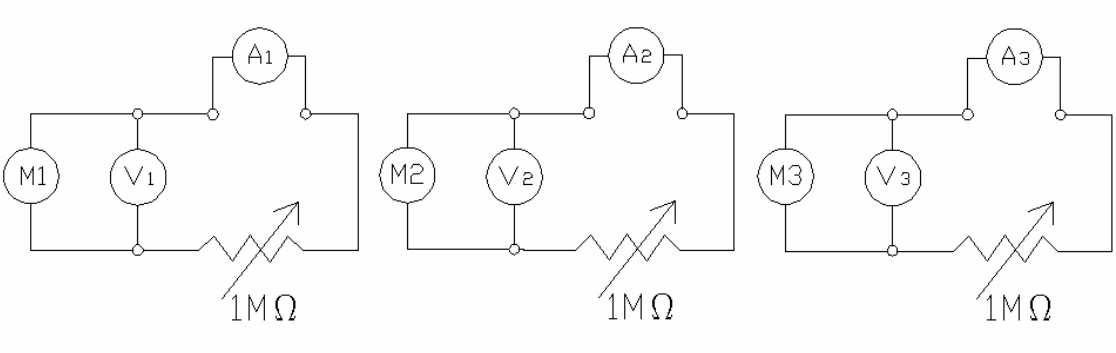

Figure 28.Circuit diagram of the array.

4.4. WATERPROOF HOUSING AND FITMENT

Once the motor and the rotor were chosen, they were coupled on with a 8mm diameter shaft. The motor and the gearbox were housed in a plastic made cylinder. As the whole system was designed to work in underwater conditions the drillings for the shaft and for the wires for the motor output were sealed with silicon.

The cylinder containing the rotor and the electro-mechanical devices was placed over a 20 cm tower made of aluminium and fixed to a $10cm^2$ basement.

The fitment for the whole model was a 20lb weight, big enough to cope with the drag force caused by the flow on the rotor.

The assembly and final appearance of the model are shown in figure 29 below:

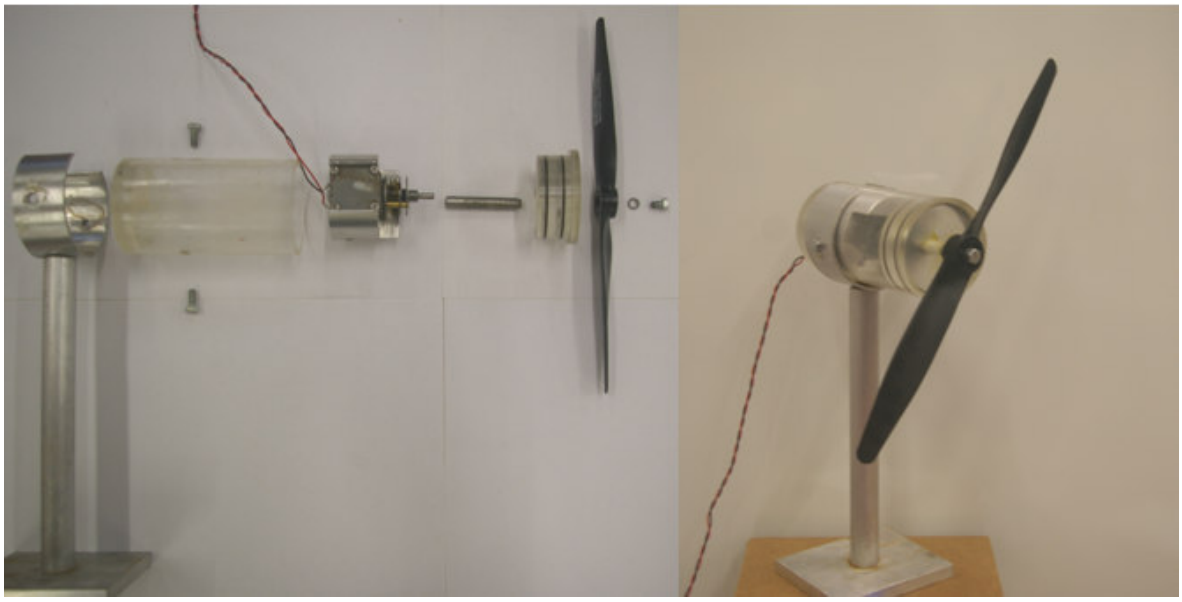

Figure 29. Marine Current Turbine model

4.5. EXPERIMENTAL TESTING

The models were tested inside the flume in order to work out their nominal values regarding both mechanical and electrical parameters.

4.5.1. Rotational speed

The rotational speed of each model was measured in order to verify the assumption made on the tip speed ratio of the rotor.

The values obtained for the model A are shown below:

Model A	
Measured flow speed	**0.39 m/s**
Measured rotational speed	**104 rpm**

Table 6. Experimentally measured speeds for model A.

According to these values:

$$104\ \frac{\text{rev}}{\text{min}} \cdot \frac{1\text{min}}{60\text{s}} \cdot \frac{2\pi\ \text{rad}}{1\ \text{rev}} = 10.9\ \text{rad/s}$$

$$v_{rotor} = \omega_{rotor} \cdot R_{rotor} = 10.9\text{rad/s} \cdot 0.125\text{m} = 1.36\text{m/s}$$

$$\text{tip speed ratio } (\lambda) = \frac{\text{tip speed of blades}}{\text{flow speed (U)}} = \frac{1.36}{0.39} = 3.5 \neq 4$$

According to the real tip speed ratio and the measured speeds the following values are obtained:

Rotor diameter [cm]	Rotor speed [rpm]	Rotor power [W]	Torque [mNm]	Torque [g.cm]
13	200.53	0.12	5.61	57.28
16	162.93	0.18	10.47	106.80
19	137.21	0.25	17.53	178.84
22	118.50	0.34	27.21	277.63
25	104.28	0.44	39.93	407.40

Table 7. Results obtained for real tip speed ratio.

As it can be seen, the theoretical speed (104.28 rpm) and the experimental one (104 rpm) match for the 25 cm rotor.

The speeds measured for the other two models, B and C, are shown in table 8x below:

	Model B	Model C
Measured flow speed	0.39 m/s	0.39 m/s
Measured rotational speed	107 rpm	100 rpm

Table 8. Experimentally measured speeds for models B and C.

The small differences in terms of measured rotational speed between the three models are due to small differences owing to the manufacturing process, especially lack of alignment between the motor shaft and the drilling through which it is connected to the rotor. However, they are that small that the three models can be assumed to perform identically in terms of tip speed ratio and hence rotational speed.

4.5.2. Voltage in open circuit

The nominal voltage each model was generating when working in open circuit was measured under the same flow speed conditions.

The values obtained from each model are shown in table x below:

	Voltage [V]
Model A	0.95
Model B	0.9
Model C	0.7

Table 9. Open circuit voltage values for models A, B and C.

Again the small differences between the values are due to the slightly different rotational speeds previously recorded.

4.5.3. Voltage and current in closed circuit

The voltage and current in closed circuit were measured at the maximum flow speed given by the pumping system of the flume: 0.47 m/s.
The reason for this is the array configurations with the loaded turbines will be analyzed under this flow speed, in order to obtain the maximum power from the turbines and be able to play with a wider range of electrical loads.

The highest current given by the models was 120 mA at a voltage of 0.8 V, giving a power of 96mW.

Assuming the value of 0.3 for the Cp, the available energy from the flow for the 25 cm rotor diameter was 0.67 W, so the efficiency of the whole electro-mechanical system would be:

$$\eta = \frac{0.096}{0.67} \cdot 100 = 14.4\%$$

5. EXPERIMENTAL SIMULATION

5.1. WAKE CHARACTERIZATION

The wake each model is going to produce downstream of its position will be one of the key factors when analysing the performance of the whole array.
As there are some small differences between the three models, they were separately tested inside the flume in order to characterize the wake each of them was producing.

The array configuration which is being studied in this piece of work assumes each of the models within the array performs identically in terms of energy production and wake effects. As we saw in section 4.5, there were some differences in terms of energy production due to small differences during the manufacturing process, subsequently, there might be some differences in the wake each model will produce. Owing to this, the three models were separately tested inside the flume.
This separate characterization will be a main factor when analyzing the performance of the whole array in case some differences are found between the three wakes, as these differences will have to be considered in order to work out an accurate analysis of the wake effect within the array.

5.1.1. Settings

- Model

Each of the models was placed in the middle of the flume and fixed with the 20 lb weight at a distance of 10 m from the water inlet.

- Flume

The flume was filled with water and the pumping system was fixed at 25% of its capacity, giving a flow speed of 0.4 m/s and a water depth of 40cm.

- Velocity Meter

The velocity meter employed during this work was a Nortek Vectrino version 1.26.
This velocity meter measures the speed of the water by using the Doppler Effect, transmitting a short pulse of sound and then listening to its echo in order to get the change in frequency of that echo.
The sound does not reflect from the water itself, but from the suspended particles in the water which circulates along the flume.

The components of the Vectrino velocity meter are described below:

Probe: the probe is mounted on a rigid stem connected to the main housing and it is made of titanium. It consists of four receivers, each mounted on a steel arm and covered with a hard epoxy, and a transmitter which is located between the four receivers.

Main housing: the main housing is a plastic cylinder which contains the electronic module, with the power transmitter, the analogue and digital signal processor, the power conditioner and the data recorder.

Power and communication cable: the power and communication cable is connected to the main housing and supplies DC power at 12-48 V and connects the Vectrino with an external computer by a 2-way serial port.
These components can be seen in figure 30 below:

Figure 30. Vectrino components

The Vectrino velocity meter transmits the short pulse of sound through a central beam emitted by the transmitter and receives four beams through the receivers. The five beams intersect at approximately 50 mm from the transmitter, where the sampling volume is located. The sampling volume is cylinder shaped and that is where the three components of the water speed, x, y and z are measured.

The sign convention of the velocity meter inside the flume is shown in picture 31 below:

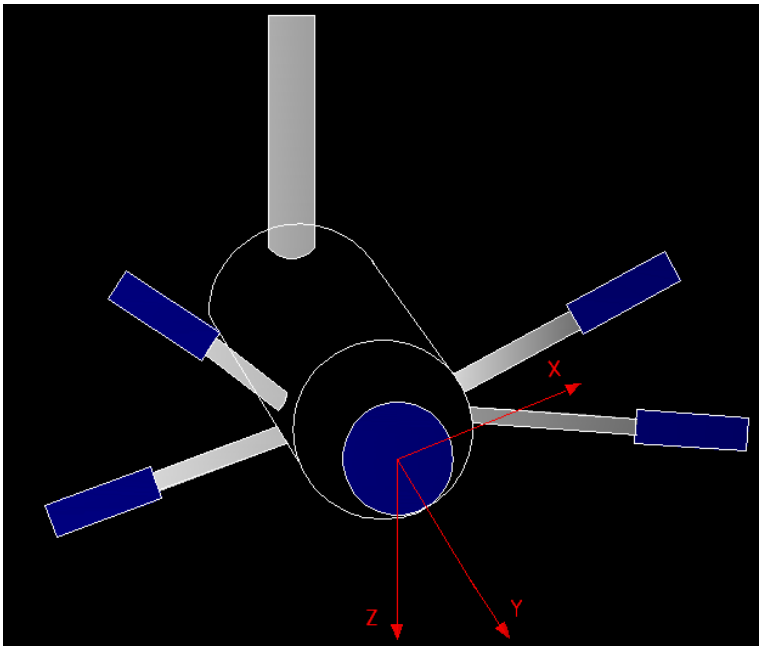

Figure 31. Sign agreement of the velocity meter.

Technical data (values selected for this application):

Water velocity measurement

Range: ± 0.1 m/s

Accuracy: ± 0.5% of measured value ± 1mm/s

Sampling rate: 50 Hz

Sampling volume

Distance from probe: 0.05 m

Diameter: 6 mm.

Height: 2.5 mm.

Echo intensity

Acoustic frequency: 10 MHz

Resolution: 0.45 dB

Dynamic range: 60 dB

The velocity meter was placed at different points in the same cross-sectional area every 25 cm, i.e. at each rotor diameter, until a distance of 2.75 m. (11 rotor diameters) downstream of the turbine.

In order to keep the velocity meter steady in a vertical position at each point, so movement-induced noise could be avoided, the device was fixed on a support above the flume by using two clamps. The support was provided with two wheels fitted into lanes so it could be smoothly moved along the flume allowing the velocity meter to be easily placed at each different rotor diameter once its position was fixed for each different sampling point.

The setting of the velocity meter is shown in figure 32 below:

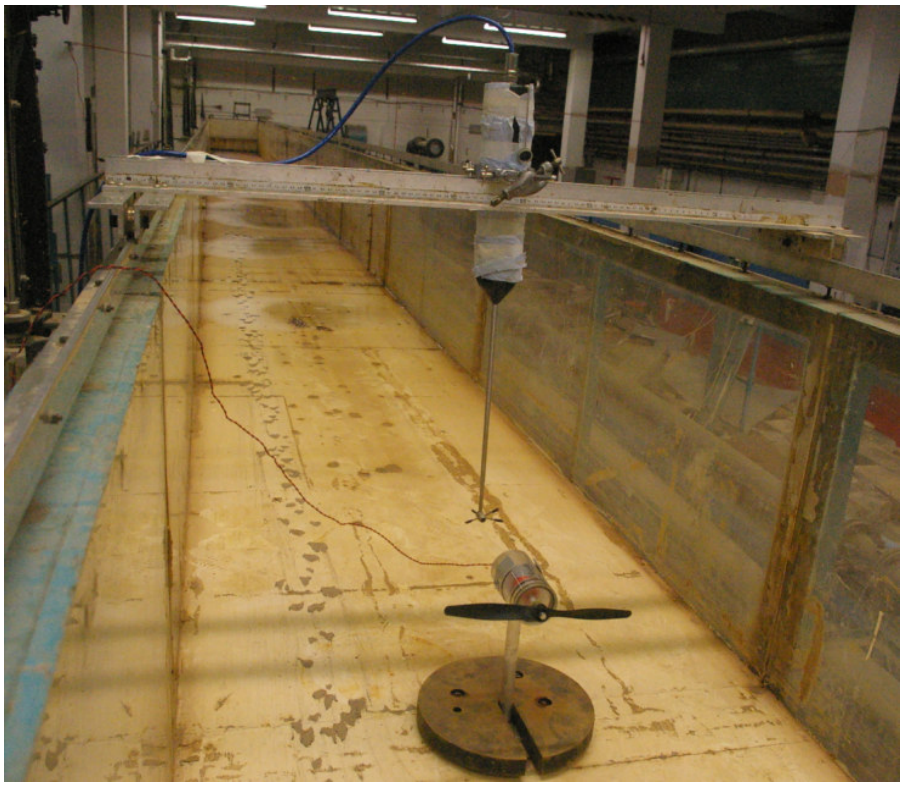

Figure 32. Velocity meter setting.

5.1.2. Samples

Different measurements of the flow speed downstream of the model were taken in order to characterize the wake produced by the turbine.
As was previously explained, the velocity deficit caused by the turbine extracting energy from the flow should bring lower downstream flow speeds than the inflow speed upstream.
Three different components of the flow speed were measured: x, y and z, with "y" being the main component, i.e. the speed in the direction of the flow.

Taking into account this sign and that convention the velocity meter will be placed inside the flume as shown in picture x above (photo), the main component of the flow speed - "y" -, will be negative in all the values taken during the measurements, however, the sign will be neglected when working out graphs and discussions in order to make the analysis easier.

- Points

The flow speed was measured at 11 different points of the cross-sectional area at each rotor diameter.
9 points were located in the swept area of the turbine, measuring the speed in the centre of the wake (point 0), in the middle of the blade (points 1R, 1L, 1U and 1D) and at the tip of the blade (points 2R, 2L, 2U and 2D) as shown in figure 33 below:

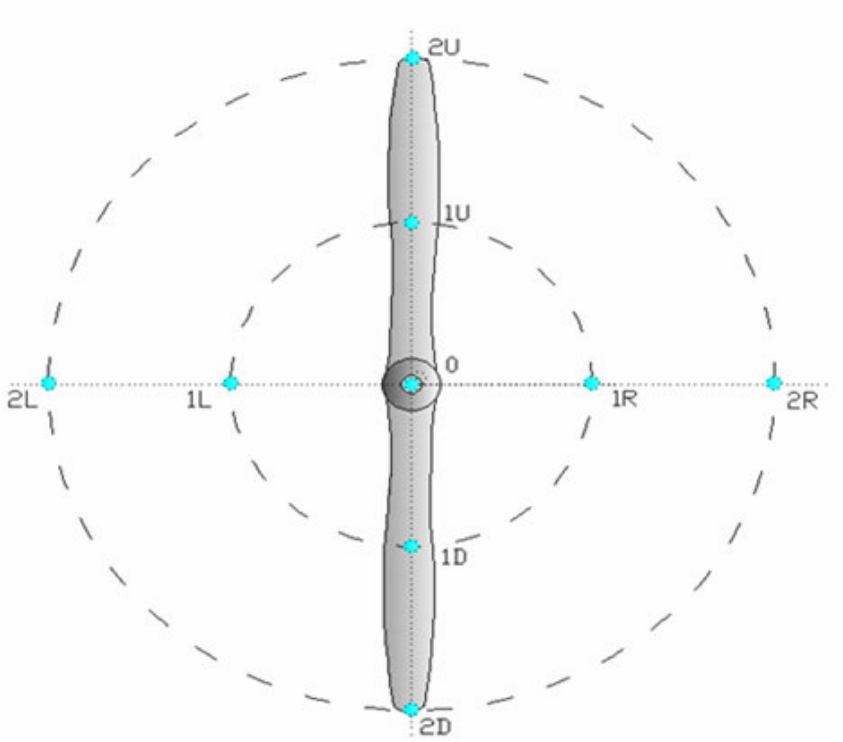

Figure 33.Sampled points in the swept area at each rotor diameter.

2 other points were located on the sides of the swept area at a distance of 1 rotor diameter from the centre of the hub (points 1RDR and 1RDL). The whole distribution of sampling points is shown in figure 34 below:

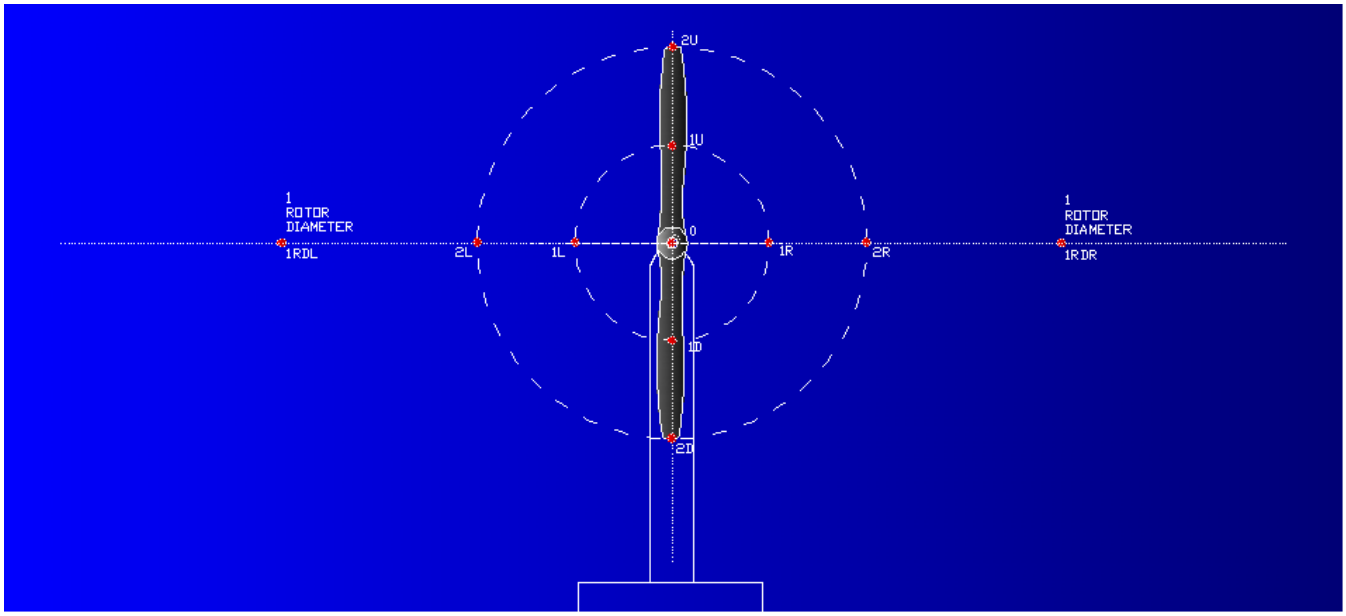

Figure 34.Sampled points in the cross-sectional area of the flume at each rotor diameter.

5.1.3. Results

- Point 0

The velocity recovery profile at this point is shown in figure 35 below for the models A, B and C:

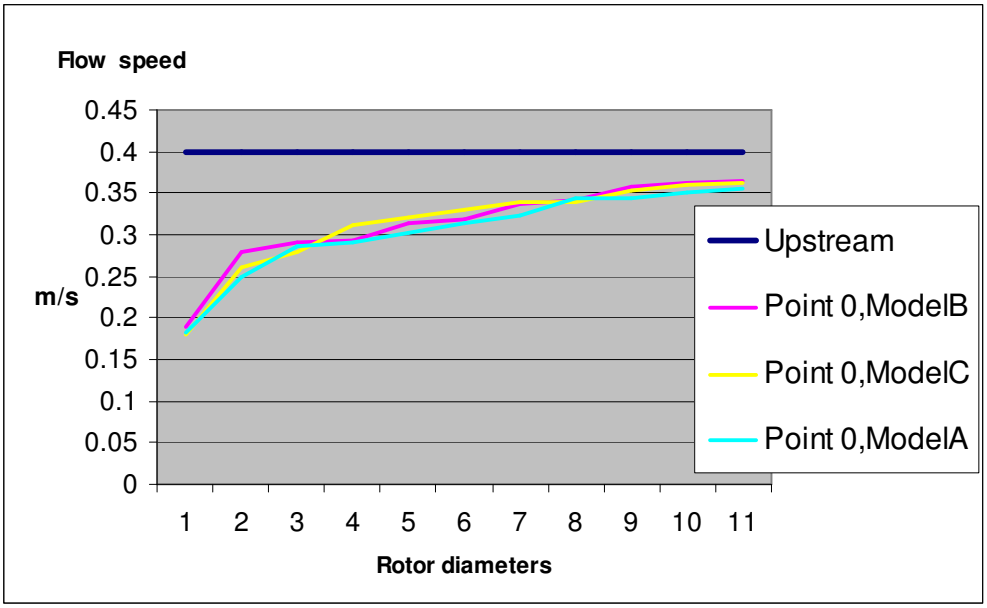

Figure 35. Velocity recovery profiles at point 0.

As seen in the graph, the three models show a clear recovery profile. The flow speed was reduced to about 45 % of the upstream flow at 1 rotor diameter, and then it recovered steadily until it reached a steady state of approximately 90 % of the upstream flow speed at about 11 rotor diameters from the device.

It should be noted that the speed recovered more rapidly during the first and second rotor diameters, probably due to the hub effect.

These results are quite similar to those obtained in [5], where the wake characterized was produced by a mesh disc of 10 cm diameter, regarding the trend of the velocity recovery profile in the centreline, with flow speeds being a mean value of 8% higher at 3, 6 and 9 rotor diameters. The reason for this, apart from the difference in size, could be that, in our case, the energy is extracted as mechanical motion while the mesh disc just converts it into turbulence downstream.

This graph shows that the three models can be assumed to perform in a very similar way in terms of wake production, hence, the characterization of the wake was carried out just for model A from this point on. The other two models should present exactly the same wake as that one.

- Points 1R and 1L

The velocity recovery profile at these points is shown in figure 36 below for model A:

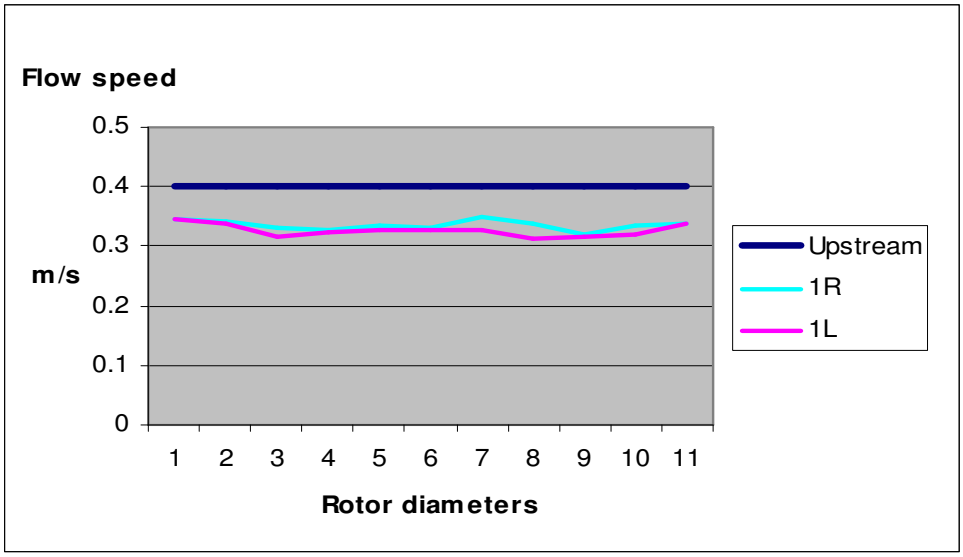

Figure 36. Velocity recovery profiles at points 1R and 1L.

As expected, the points located in symmetrical positions in the swept area of the rotor have almost identical recovery profiles. However, at these points not only there is no appreciable recovery, but also flow speeds seem to decrease during the first rotor diameters. The overall speed at both locations could be considered as steady around a value of 0.34 m/s (85 % of the upstream flow speed) all along the downstream distance.

The reason for this lack of recovery might be the constraints from the walls, which apparently make the wake persist all along the measured distance.

- Points 2R and 2L

The velocity recovery profile at these points is shown in figure 37 below for model A:

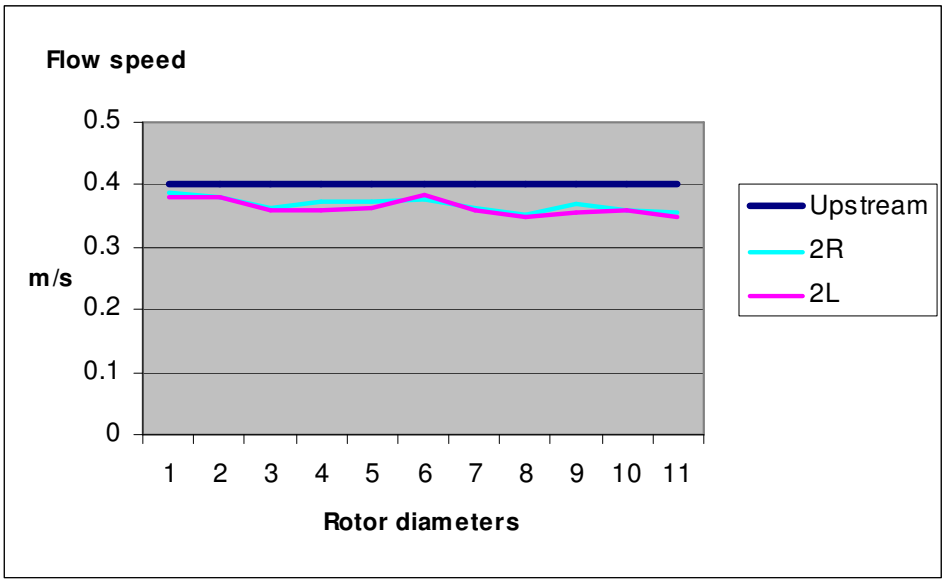

Figure 37. Velocity recovery profiles at points 2R and 2L.

Again no recovery profile was recorded, however, some interesting aspects can be noted from the graph.

The flow speed remains constant at a value of 0.38 m/s (95 % of the upstream flow speed) almost until the second rotor diameter, and then it starts to drop, this could be due to the expansion of the wake. According to that, points 2R and 2L would stay right on the edge of the wake during the first rotor diameter, and hence keeping almost the upstream flow, then, the expansion of the wake would make the points be more inside the wake, reducing their flow speed.

Apart from that, it can be clearly seen that both trends have an average speed of about 0.36 m/s (90 % of the upstream flow speed), which is higher in comparison with the points measured in the middle of the blade (points 1R ad 1L). This could be explained by the proximity of points 2R and 2L to the free stream flow, which would enhance fluid mixing increasing the flow speeds.

- Points 1U and 2U

The velocity recovery profile at these points is shown in figure 38 below for model A:

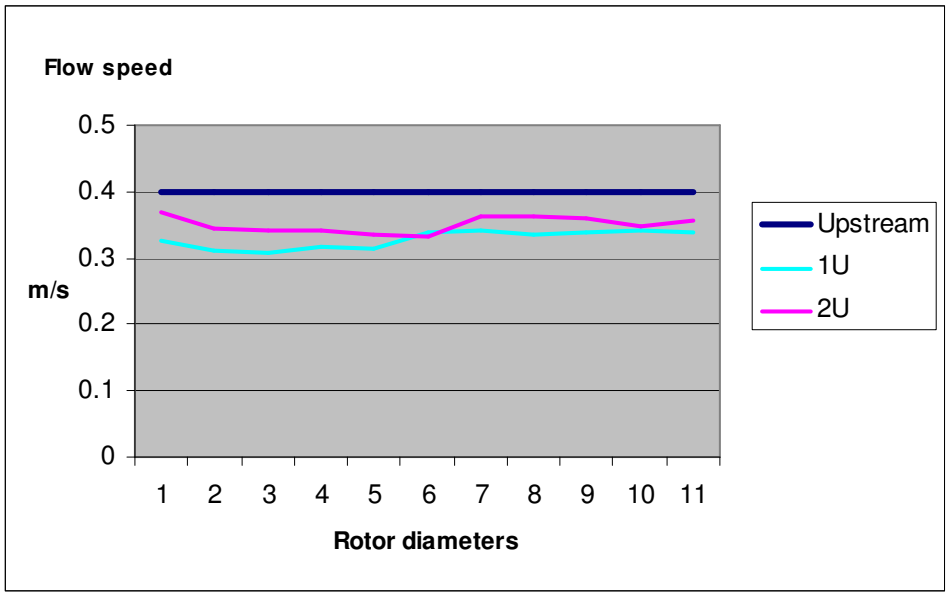

Figure 38. Velocity recovery profiles at points 1U and 2U.

No recovery was either found in the upper section of the wake. Both trends present similar average flow speeds to those at the previous points measured, around 0.35 m/s (87 % of the upstream flow speed). It can be seen how the point closer to the water surface presents as expected a higher average flow speed. Although the wake would not be allowed much vertical expansion due to the proximity to the water surface, the initial value of the flow speed for the point 2U (0.37 m/s) and the way it drops during the first rotor diameters could be also due to the expansion of the wake, which would bring the point more inside it.

- Points 1D and 2D

The velocity recovery profile at these points is shown in figure 39 below for model A:

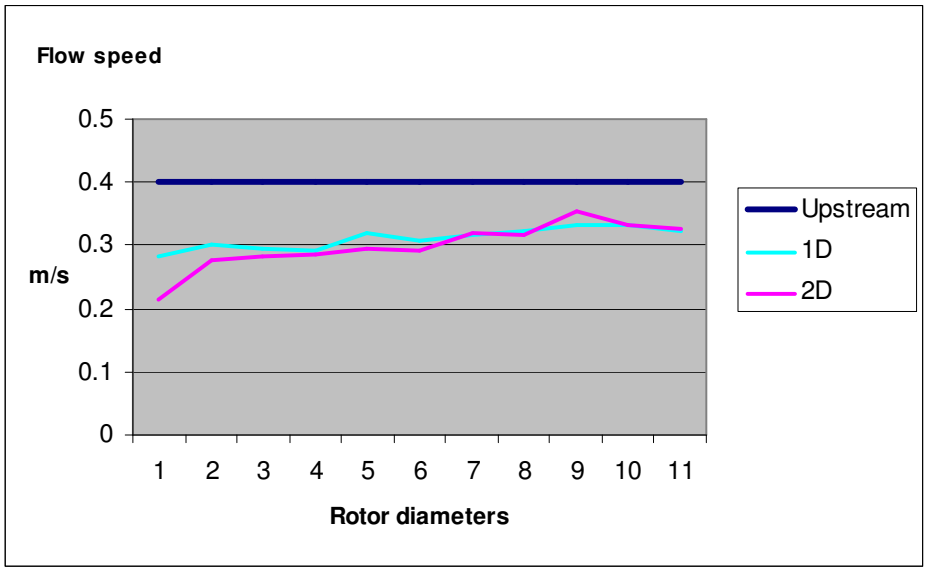

Figure 39. Velocity recovery profiles at points 1D and 2D.

As can be seen in the graph, the bottom section of the wake presents a slight recovery profile at both points 1D and 2D. This recovery is actually more significant at the point matching with the very bottom of the swept area, going from 0.22 m/s (55 % of the upstream flow speed) to 0.33 m/s (83 %), where both trends reach the steady state.

- Points 1RDR and 1RDL

The velocity recovery profile at these points is shown in figure 40 below for model A:

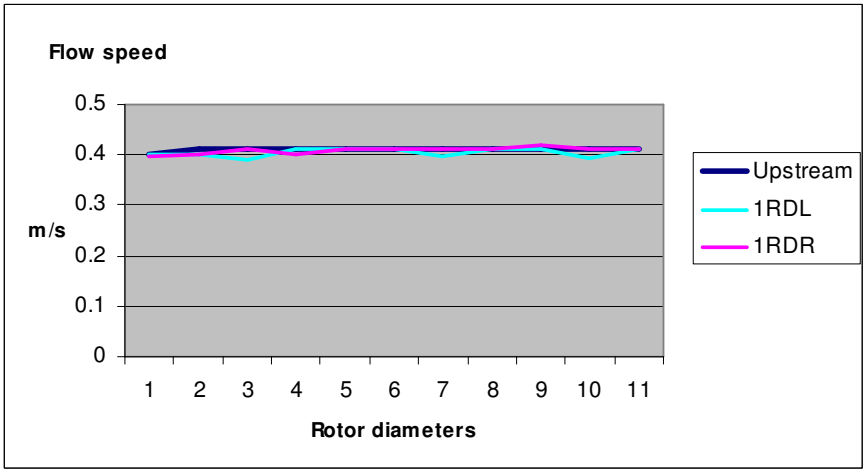

Figure 40. Velocity recovery profiles at points 1RDR and 1RDL.

The flow velocity profile in both point 1RDR and 1RDR shows there was no alteration of the upstream flow, as the value of 0.4 m/s was maintained during the whole measured distance with no variation but that from water turbulence. This shows that the wake produced by the turbine was quite constrained during the whole distance downstream, probably due to the narrowness of the flume, and, if there was any expansion, it stopped before reaching a lateral distance of 1 rotor diameter.

A gradient graph of the flow speed at 3, 6 and 9 rotor diameters is shown for each of the three components - X, Y and Z- measured at the 9 sampling points previously detailed, is shown in figure x below.
Due to the low density of sampling points, the interpolations carried out show very sharp areas, however, and even without the possibility of doing a detailed analysis, some interesting findings can be drawn from the graphs:

The three graphs of the X component show two well differenced sections: an upper half section with negatives values of the speed, and a lower half section with positive values, taking into account the absolute value of the speeds is very similar in both sections, the graph is showing the rotation of the wake in the X-plane, which makes sense taking into account the sign convention of the velocity meter and the fact that the turbines were rotating anticlockwise.
A similar effect can be observed in the graphs of the Z component, with the flow going down in the left half section of the graph. However, the flow does not seem to go up in the right half section of the graph because no negatives values are appearing, however, flow speeds are lower than in the other half section probably due to some components going also down in the right one.
The three graphs of the Y component (negatives values are due to the sign convention of the velocity meter) show how the flow recovers mainly in the core and in the outer sections of the wake. We can also note some kind of bottom effect, with big flow decay until about 6 rotor diameters in the down line of the wake.

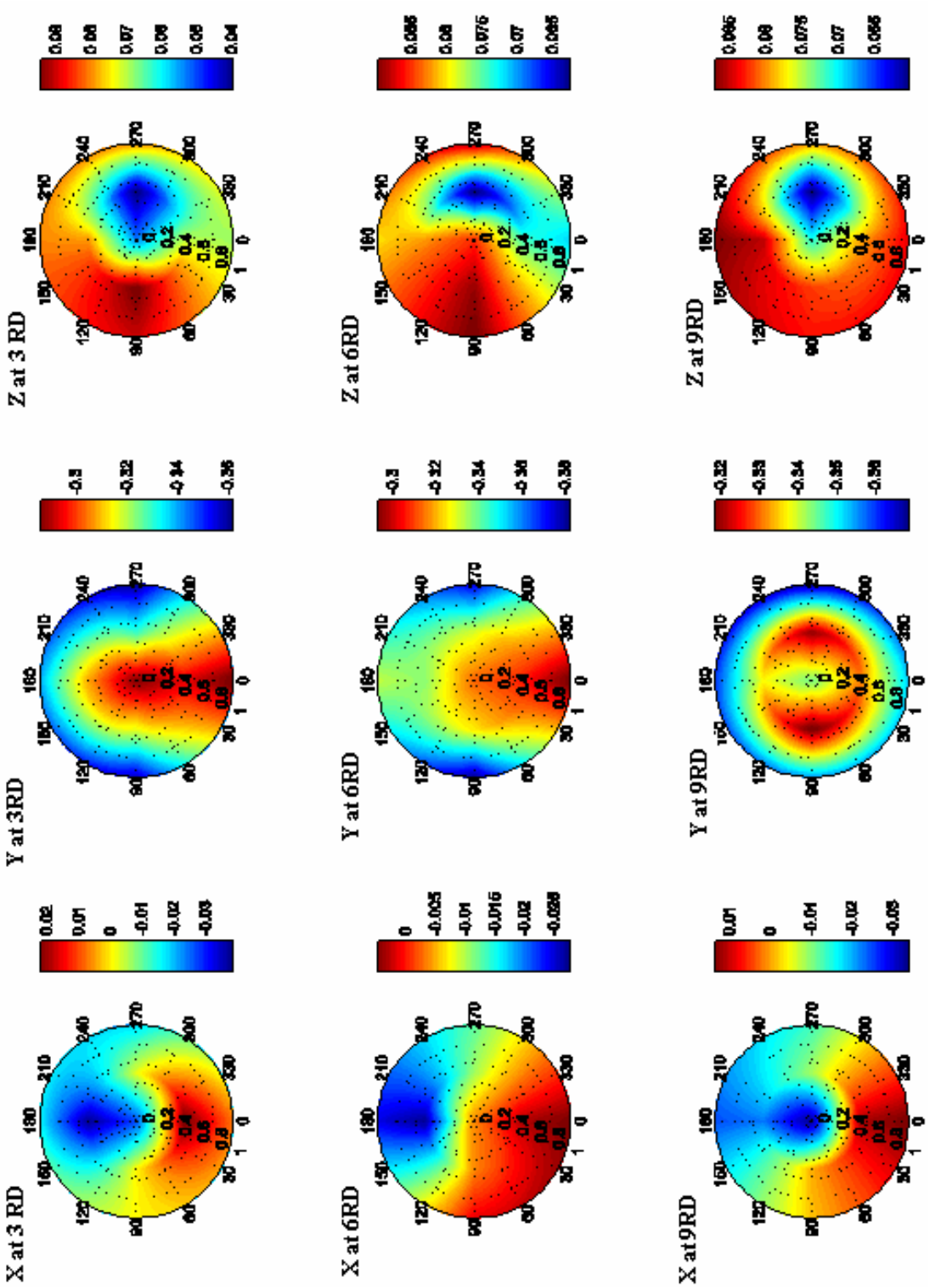

Figure 41. Polar contours of the flow speed at 3, 6 and 9 rotor diameters.

5.2. ARRAY ISSUES

5.2.1. Configurations

The performance of the turbines was analyzed in different array configurations in order to find out how the array effects were affecting the output of the turbines.

Two main configurations were analyzed in this piece of work, and as only three models were manufactured, both configurations were made up of only two rows of devices, however, this array density was actually enough to analyze how the turbines were affected by the other surrounding devices.

Configuration 1 consisted of one turbine in the first row of the array (turbine A) and two turbines in the second row of the array (turbines B and C), and Configuration 2 consisted of two turbines in the first row (turbines A and B) and one single turbine in the second row (turbine C). The layout of these two configurations is shown in figure 42 below:

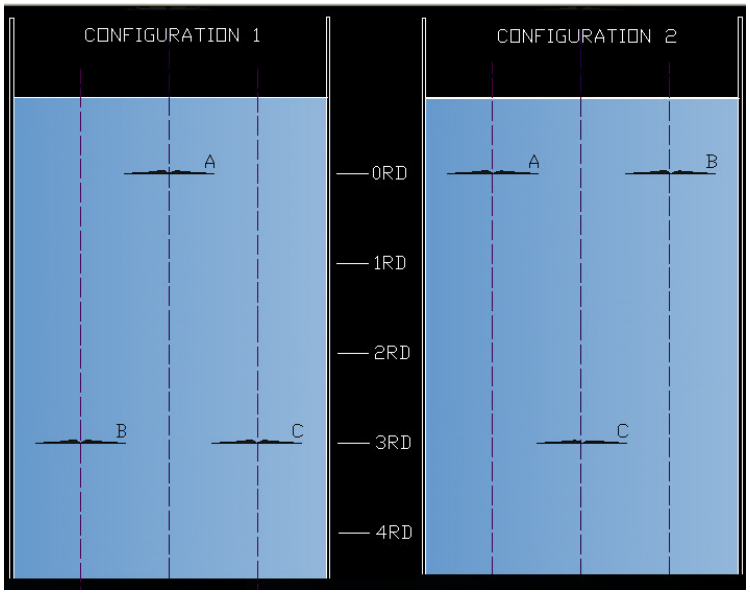

Figure 42. Main array configurations.

In addition to this, different variations of each configuration were also analyzed. There were basically two key factors considered when varying the layout of the

configurations. On one hand the lateral spacing of the turbines and on the other hand the longitudinal spacing of the rows.
By varying these factors, 6 different combinations of each configuration were considered:

In configuration 1, three different positions of the turbine in the first row were tried, and each of those three positions was tried for three different longitudinal spacing of the second row of turbines.

In configuration 2, three different lateral spacings between the turbines in the first row were tried, and each of those lateral spacings was tried for three different longitudinal spacing of the turbine in the second row.
The different combinations were named using a numerical notation. This consists of numbers separated by hyphens. The first number indicates the configuration (1 or 2), the second number indicates the variation of that configuration regarding the lateral spacing of the turbines, and the third number indicates the number of rotor diameters separating the two rows of the array (3, 6 or 9).

The different lateral spacing indicated by the second number of the notation is described below and illustrated in figure 43:

Configuration 1:
Second number = 1, turbine A is in the centre line of the second row of turbines
Second number = 2, turbine A is in the line of the tip of the blade of turbine B.
Second number = 3, turbine A is in the same line as turbine B.

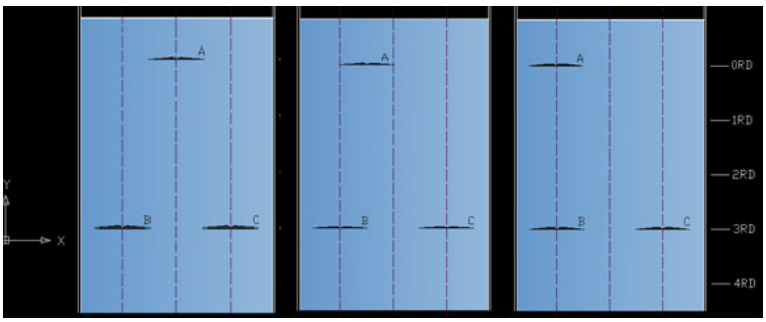

Figure 43. Different locations for turbine A in configuration 1.

Configuration 2:

Second number = 1, turbines B and C are separated 2 rotor diameters.
Second number = 2, turbines B and C are separated 1.5 rotor diameters.
Second number = 3, turbines B and C are separated 1 rotor diameter.

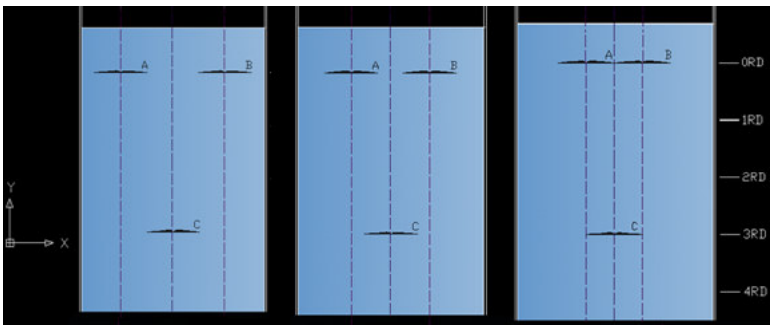

Figure 44. Different lateral spacings in configuration 2.

So, the combination 2-2-3 would be two turbines in the first row separated 1.5 rotor diameters and one turbine in the second row separated 3 rotor diameters from the first row.
Due to the narrowness of the flume, it was actually impossible to evaluate more realistic values of lateral spacing (around 3 rotor diameters) between the turbines in a same row, however, the effects of placing the turbines very close one to each other, even as close as just one rotor diameter – a configuration which matches with the concept of a tidal fence – is also very interesting.

5.2.2. Loading of the turbines

In order to evaluate how the presence of an electrical resisting torque was affecting the performance of the turbines, the arrays were analyzed under different loading conditions.

- Unloaded array

In this situation the different array configurations were analyzed with the turbines working in open circuit, i.e. no energy production was being carried out, so the voltage output from the turbine was the magnitude used to evaluate the array effects.
The performance of each turbine was then shown as a percentage of its nominal value [V_n].

The nominal value of each turbine is defined in this piece of work as the output voltage given by the turbine when powered by the free upstream flow, i.e. the output voltage of the turbine without the influence of other devices.

Instead of using the same speed of the flow as in the wake characterization and the experimental testing of the model, 0.4 m/s, the speed of the flow when simulating the array was increased to 0.47 m/s for the turbines to give a higher output, so the nominal values obtained were obviously higher than those recorded in the Model Definition/Experimental Testing section.
However, due to some problems derived from the underwater conditions in which the turbines were working, such as rusting and condensation in the gearboxes, the mechanical resisting torque of the turbines was not the same during the length of the project.
Because of this, the turbines were tested before measuring each configuration in order to accurately find out and update their nominal values, so no difference in the performance of the turbines could be attributed to the array effects by mistake.
The nominal values for each configuration are shown in table 11 below:

	Nominal Values [V]	
	Configuration 1	Configuration 2
Model A	**0.85**	**1.2**
Model B	**1.2**	**0.85**
Model C	**1.2**	**1.3**

Table 11.Nominal voltage values for each configuration

- Loaded Array

In this situation the turbines were meeting an electrical resisting torque in a closed circuit, and hence producing electrical energy. The performance of the turbines was then analyzed taking into account their power output and calculating their array efficiency, based on the power output of the turbines without the influence of other devices, as explained in section 3.1.

Although the maximum power given by one turbine was 96 mW, as shown in the Model Definition/Experimental Testing section, not all the turbines were able to reach that output. In this case, as the output of the turbines was fixed by controlling their loads through the potentiometers, the nominal values were not subject to changes because of environmental conditions. The values fixed before the measurement of each configuration are shown in table 12 below:

	Nominal Values [mW]	
	Configuration 1	Configuration 2
Model A	**76 or 47**	**85**
Model B	**85**	**85**
Model C	**85**	**81**

Table 12. Nominal power outputs for each configuration.

Each of the two array configurations was analyzed in a different way when the turbines were loaded.

Configuration no.1 was analyzed with some variations, which consisted on varying the load of turbine A (the one located in the first row). Two different loads were tried, 2Ω and 12 Ω, with turbine A giving 76 and 47 mW respectively. This was done with the intention to prove that a higher energy extraction from the flow would lead to an increasing of the velocity deficit downstream of the turbine, affecting the performance of the devices in the second row.

Configuration no.2 was firstly analyzed keeping the three turbines A, B and C at the same loading, and hence producing a similar amount of energy. The aim of this was to find out whether there was any difference between this performance and that from the Configuration 2 when the turbines were not loaded.

5.2.3. Results

Unloaded array

- Configuration 1-1-3:

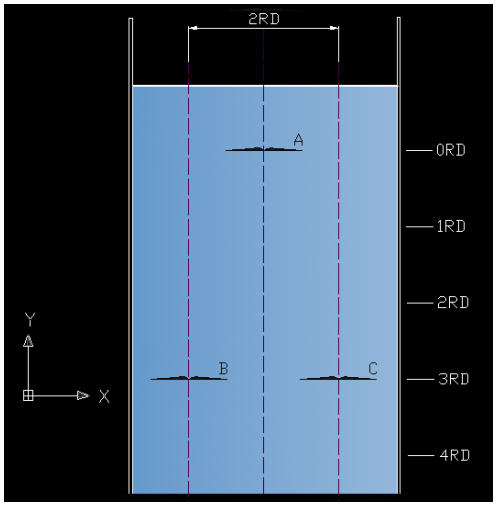

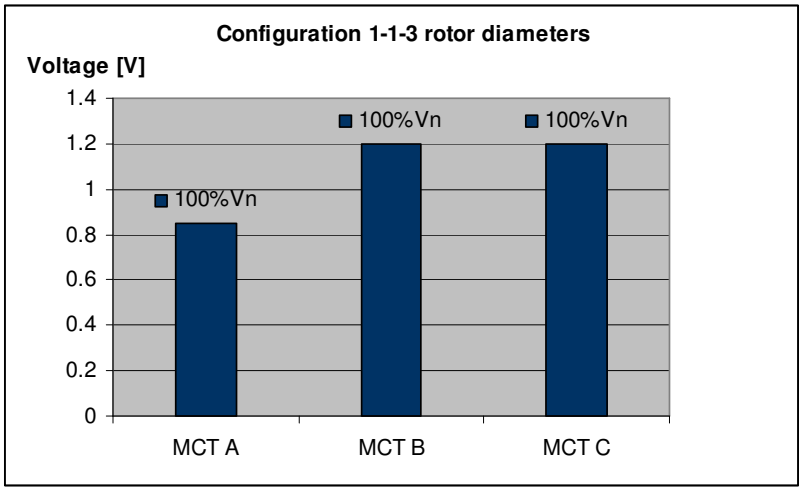

Figure 45 and 46. Array configuration 1-1 and turbine performance.

In this configuration, turbine A had no impact on the performance of turbines B and C, which kept producing their nominal output voltage. In the configurations 1-1-6 and 1-1-9 the situation was the same.

- Configuration 1-2:

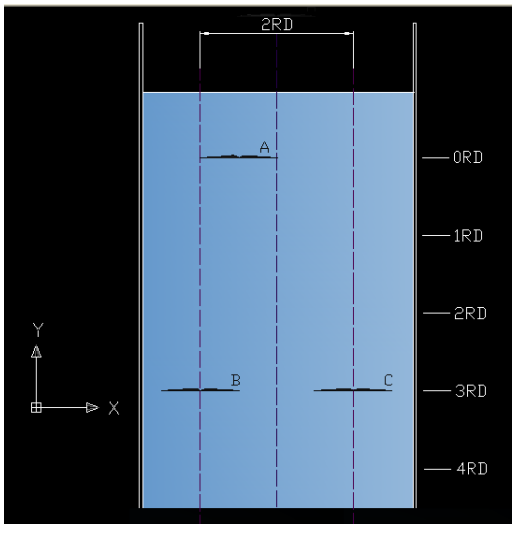

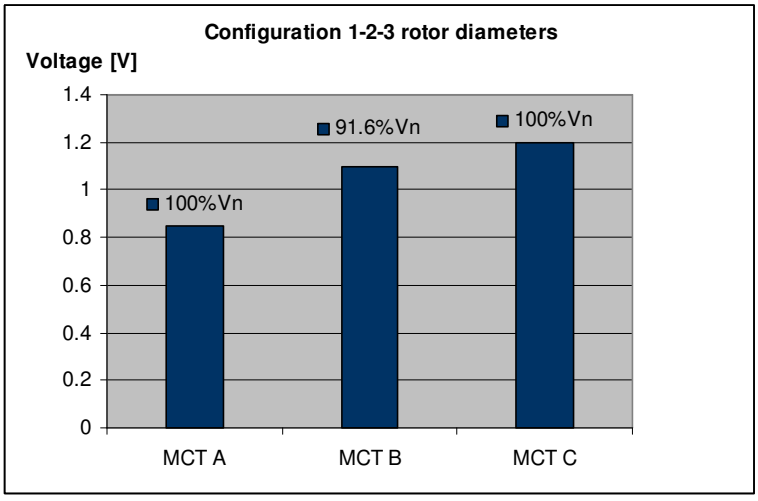

Figure 47 and 48. Array configuration 1-2 and turbine performance.

In this configuration we can see the first array effect, which affected turbine B by reducing its output voltage by 8.4 % due to the flow decay produced by turbine A. In the configuration 1-2-6, the output voltage of turbine B was again equal to the nominal one, which means the flow had recovered at that downstream distance.

- Configuration 1-3:

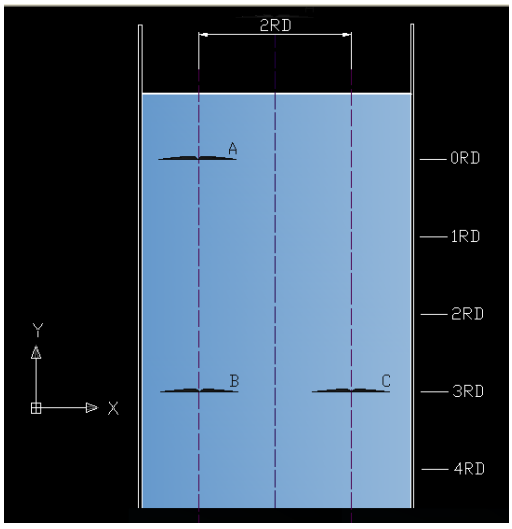

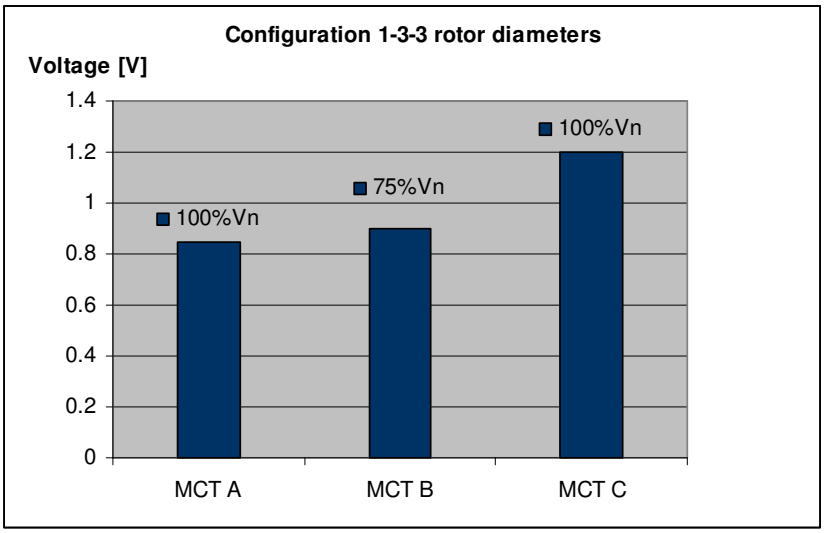

Figure 49 and 50. Array configuration 1-3 and turbine performance.

In this configuration the array effect caused by turbine A on turbine B is obviously stronger, and hence its output voltage decreased to 75% of the nominal value.
This value is quite high taking into account the flow speed of point 0 at 3 rotor diameters was reduced to 72.5% of its nominal value, however, the turbine is averaging the wake effect over a much bigger area, and the other points measured in the swept area were actually much closer to the inflow speed.

It can be seen in the next figure for the configuration 1-3-6 how the velocity recovers as the downstream distance increases, with the output voltage of turbine B increasing to 83.3% of the nominal voltage at 6 rotor diameters.
It is remarkable that this recovery trend did not continue, and the output of the turbine was still 1 V in the configuration 1-3-9, so the flow did not develop further over that distance.

- Configuration 1-3-6:

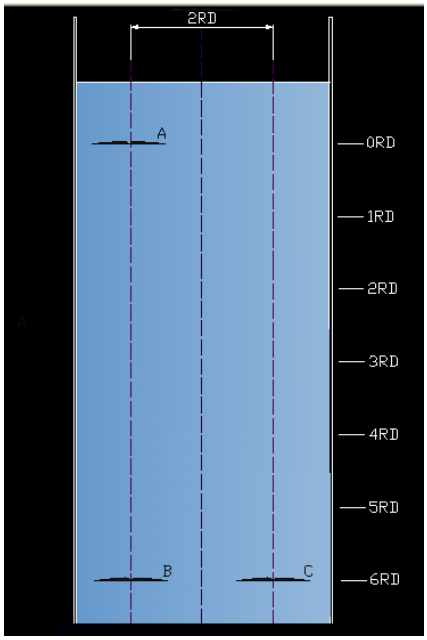

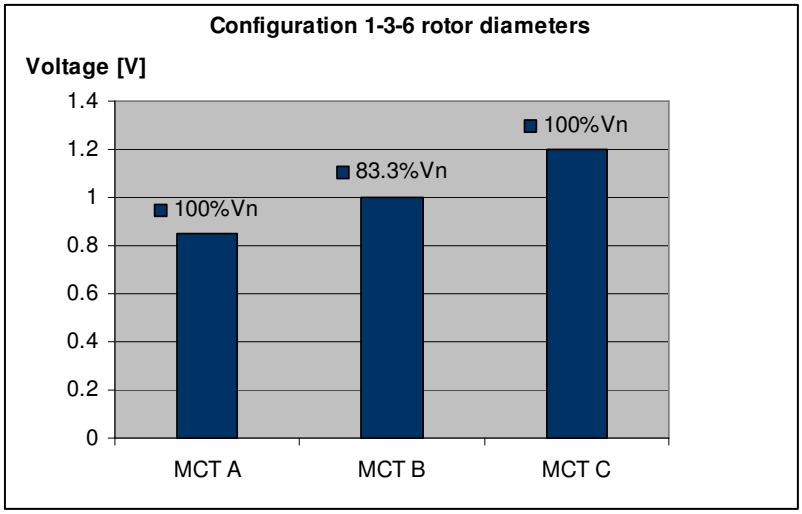

Figure 51 and 52. Array configuration 1-3 and turbine performance.

- Configuration 2-1:

The results for Configuration no.2 are shown only for turbine C, as turbines A and B obviously keep on producing their nominal voltage output for all the combinations of this configuration.

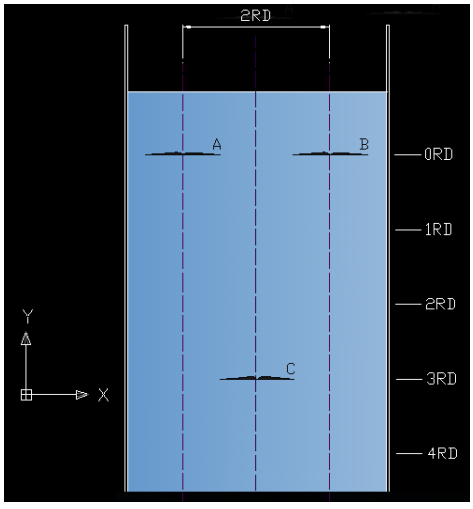

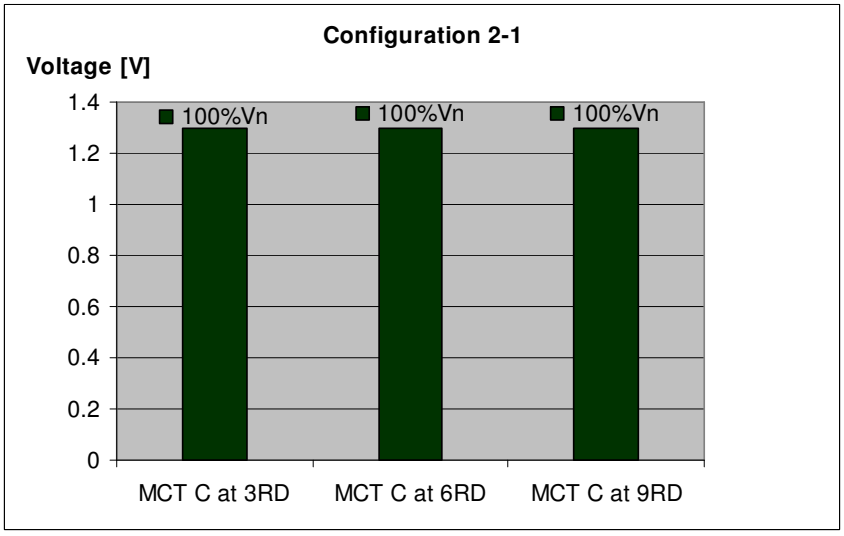

Figure 53 and 54. Array configuration 2-1 and turbine performance.

As in Configuration 1, no array effect was found in turbine C, indicating that the constrained wake produced by turbines A and B, as characterized in the previous section, never reached the swept area of turbine C. The situation was the same in configurations 2-1-6 and 2-1-9.

- Configuration 2-2:

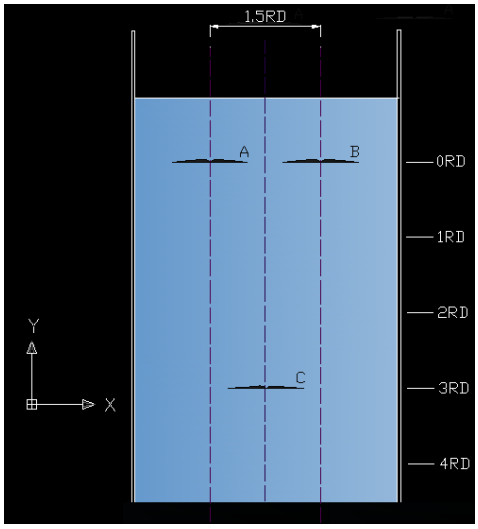

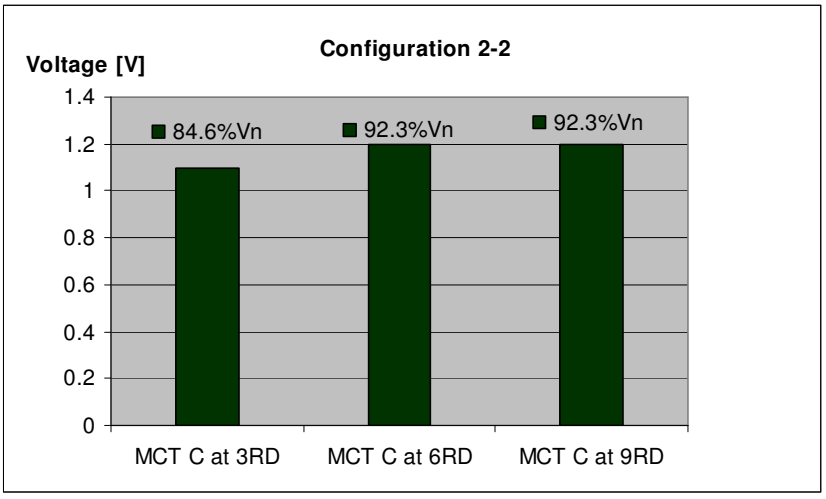

Figure 55 and 56. Array configuration 2-2 and turbine performance.

When the lateral spacing between turbines A and B decreases, the array effects start to show up as the wake reaches turbine C, reducing its output voltage to 84.6% of the nominal value at a distance of 3 rotor diameters downstream.

At 6 rotor diameters, the flow has recovered and the output voltage increases to 92.3% of the nominal value. However the flow recovery did not go any further, as the output voltage was still 1.2 V in the configuration 2-2-9.

- Configuration 2-3:

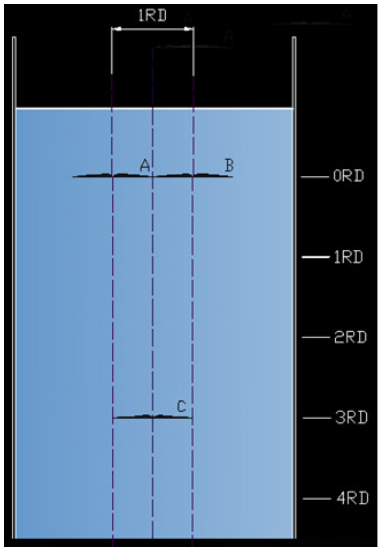

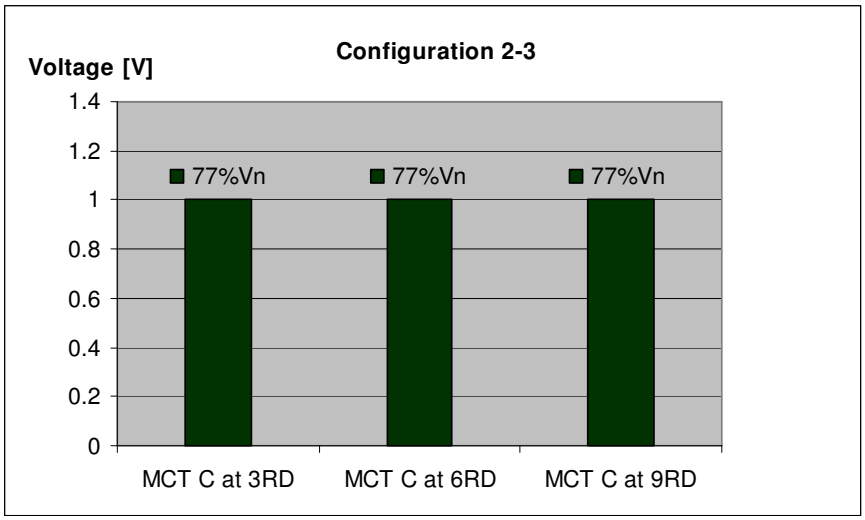

Figure 57 and 58. Array configuration 2-3 and turbine performance.

The highest output drop in the configuration 2 was found for this combination, with the turbine C giving 77% of its nominal output value. The position of the turbines in the first row make both wakes reach the swept area of turbine C, in addition to this, no free stream flow is allowed to pass between the turbines, significantly affecting the performance of the device in the second row.

In the next combinations 2-3-6 and 2-3-9, turbine C kept giving an output of just 1V, which means the combined wake from A and B persisted during the measured distance, showing no recovery of the flow.

Loaded array

Only the results for turbines B and C are shown for the Configuration no1, as turbine A, situated at the first row, remained obviously producing its nominal output value all throughout the measurements.

- Configuration 1-1:

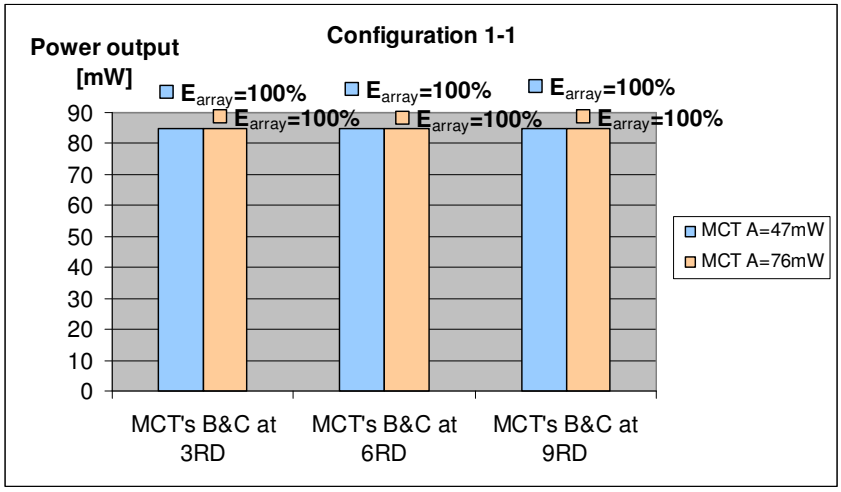

Figure 59. Turbine performance for combination 1-1.

No array effect was found in this configuration. Both turbines B and C produced their nominal output power of 85 mW during all the distances measured downstream. So again, the wake produced by turbine A did not reach the swept area of the turbines downstream for any of the loading ratios.

In the next two combinations the results will be shown for turbine B only, as turbine C did not experience any change in its output, which remained at the nominal value.

- Configuration 1-2:

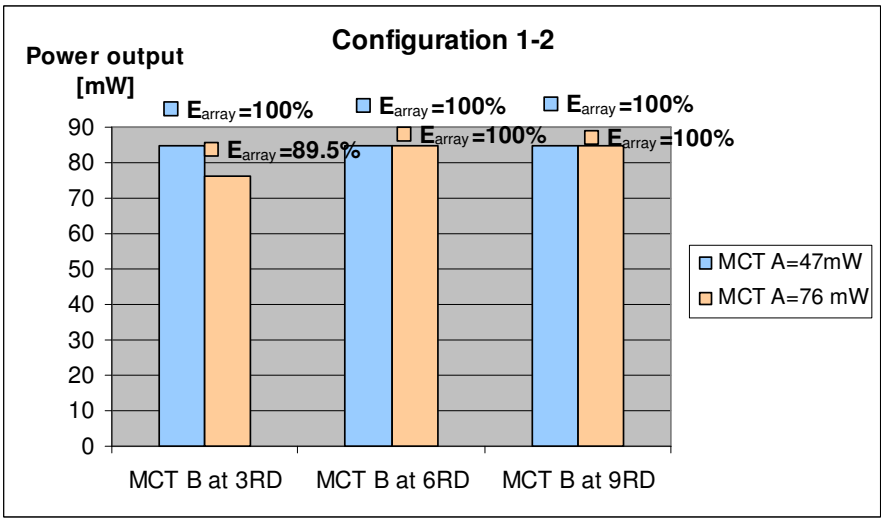

Figure 60. Turbine performance for combination 1-2.

We can see now how turbine B starts to be affected by the wake produced by turbine A, now located in the line of the tip of the blade of turbine B. Turbine B produced here a current of 80 mA at a voltage of 0.95 V, to give a power of 76 mW and an array efficiency of 89.5 %, however, this only happened when turbine A was at its highest loading, extracting 76 mW from the flow. In the same way as happened in the previous section - when the turbines within the array were not loaded - the flow recovered at 6 rotor diameters, with turbine B coming back to its nominal output value.

- Configuration 1-3:

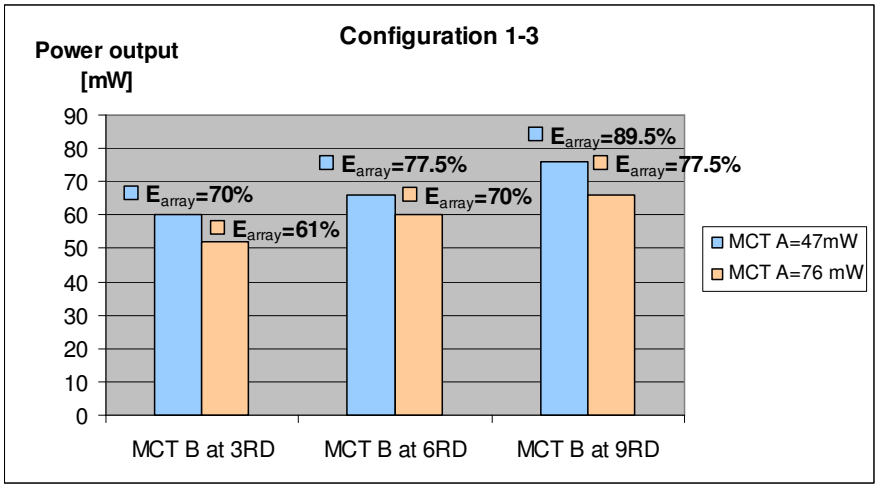

Figure 61. Turbine performance for combination 1-3.

Now turbine A is located just in front of turbine B, and the wake effects can be clearly observed in the results shown above, as well as how the different amounts of energy extracted by turbine A cause different flow decays and hence different performances of the turbine downstream.

In contrast to what was observed when the turbines were not loaded, the flow seems to keep recovering after 6 rotor diameters.

The different loadings of turbine A cause a difference of 13% in the array efficiency of turbine B at 3 rotor diameters downstream, however, is remarkable how the flow recovers almost identically after both energy extractions - basically increasing the power output between 6 and 10 mA every 3 rotor diameters- as the free stream flow reenergizes the wake produced by turbine A.

- Configuration 2-1:

The results for Configuration no.2 are shown only for turbine C, as turbines A and B obviously keep on producing their nominal power output for all the combinations of this configuration.

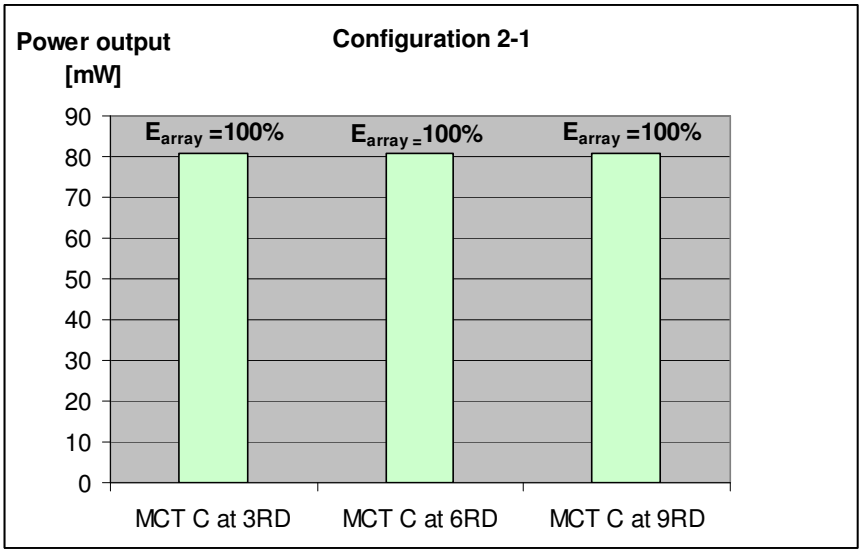

Figure 62. Turbine performance for combination 2-1.

No array effect was found in this configuration. Turbine C produced a voltage of 0.9 V and a current of 90 mA, giving a power output of 81 mW, the same as its nominal value, so the array efficiency of turbine C remained at 100% for the three different downstream distances.

- Configuration 2-2:

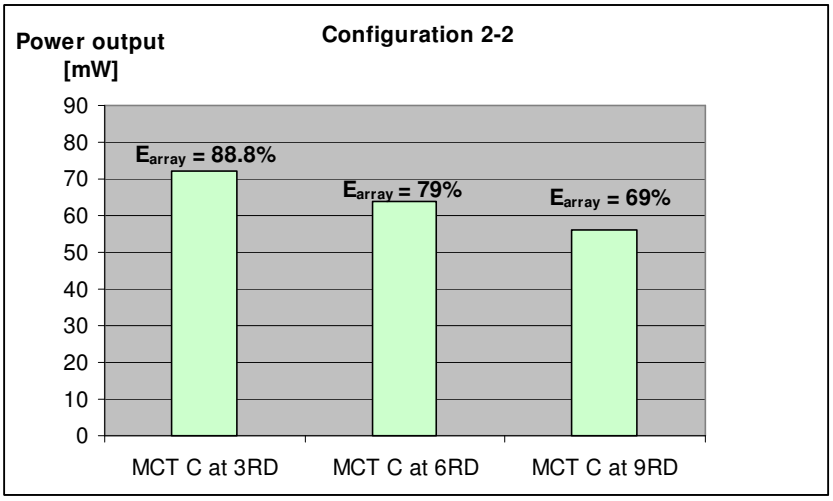

Figure 63. Turbine performance for combination 2-2.

In the configuration 2-2, with the two turbines in the first row separated 1.5 rotor diameters some interesting results were found. Turbine C produced a voltage of 0.85 V and a current of 85 mA at 3 rotor diameters, giving a power output of 72 mW and an array efficiency of 88.8 %. Surprisingly, that power output did not increase when increasing the downstream distance, as turbine C produced a power output of 64 mW at 6 rotor diameters. This pattern remained at 9 rotor diameters, with turbine C producing 56 mW.

The explanation for this phenomenon might be the expansion of the wakes produced by turbines A and B, making turbine C be more inside the combined wake at 6 and 9 rotor diameters.

Some flow speed measurements were carried out at this combination I order to clarify the results explained above. The flow speed at point 0 of the rotor swept area for the distances involved are shown in figure x below:

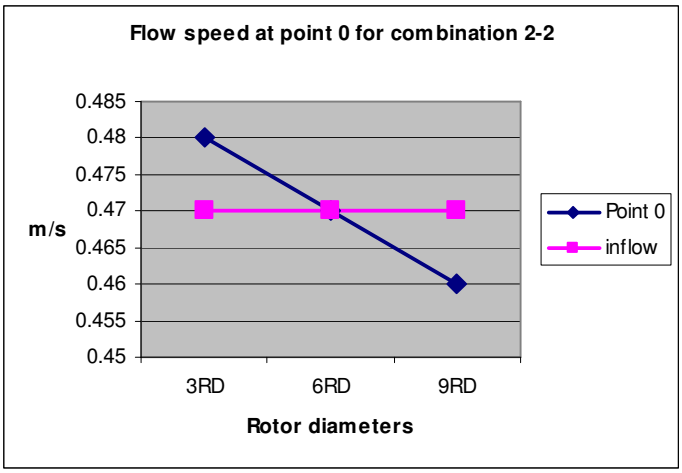

Figure 64. Flow speed at point 0 for combination 2-2.

As it can be seen, the flow speeds obtained make sense according to the power outputs recorded. The flow speed drops by 2.1% every 3 rotor diameters, so taking into account that the power is proportional to the cubed speed, the power output should drop by approximately 9.3% every 3 rotor diameters, which is pretty much the trend obtained in figure 65 below, and the difference is again due to the fact that the voltage is responding to what happens over the full swept area

It is also remarkable that the flow speed obtained at 3 rotor diameters from the first row of devices was actually higher than the inflow speed. This might be due to an

acceleration of the flow in between the two turbines of the first row as a consequence of the blockage they were producing against the flow.

- Configuration 2-3

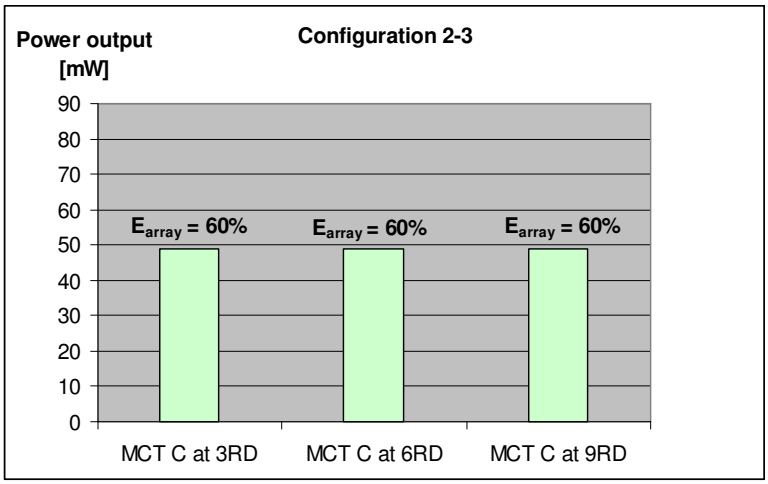

Figure 65. Turbine performance for combination 2-3.

As it can be seen in the graph, the two turbines in the first row produce very significant flow decay downstream when they are separated by just 1 rotor diameter, which results in turbine C giving the lowest output of all combinations: 49 mW at 70mA and 0.7 V, with an array efficiency of only 60%.

This power output persisted when the turbine was located at 6 and 9 rotor diameters downstream, probably due to the persistence of the combined wake and the lack of free stream flow passing through, not allowing the flow to recover from the energy extraction carried out in the first row.

- Configuration 2-3-extra.

In this case, an extra positioning of turbine C was investigated in order to analyze the possibility of the flow being diverted due to the blockage produced by turbines A and B, as shown in figure x below:

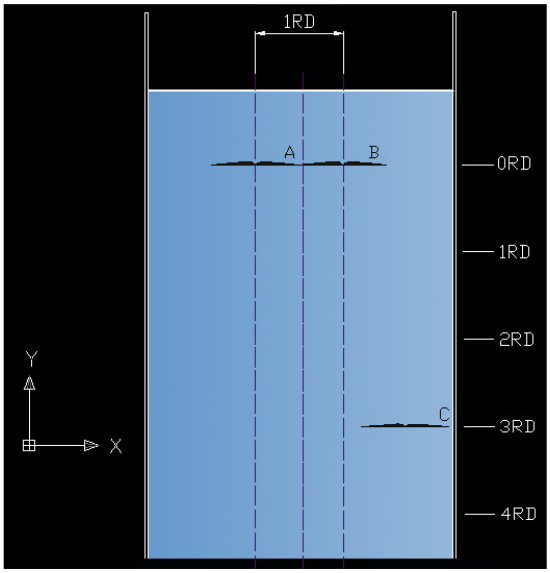

Figure 66. Extra positioning of turbine C in configuration 2-3.

In that position, turbine C produced a voltage of 0.75 V and a current of 75 mA giving a power output of 56 mW, 14.3% higher than when the turbine was placed in the centre line at the same downstream distance. This phenomenon could be then due to the flow being diverted by the turbines and constrained between the array and the wall of the flume, accelerating it.

The speed of the flow was measured at this point giving a value of 0.476 m/s, slightly higher than the upstream flow.

NOTE:

It has been quite a challenging task in this piece of work to get accurate data due to the very small scale of the models used. The small magnitude of the voltage and power measurements, in the range of 0.8 – 1.4 V and 40 – 90 mW, made it difficult to extract reasonable conclusions. However, and attributing some unexpected results to this unavoidable and very low range of the magnitudes considered, we can say array effects were significantly appreciated in the results obtained.

6. CONCLUSIONS

- Regarding array configurations

After analysing the results obtained in this piece of work, we can say that configurations 1-1 and 2-1 would be the most suitable in order to reach the target of minimise array effects and optimize the energy production, heading for an array efficiency of 100%.

However, due to the narrowness of the flume and the expectation of a more significant wake expansion at higher scales, more lateral spacing between the devices in the same row should be considered. This way, a higher rate of free stream flow would be allowed to pass through, recovering the wake. This recovery - considering the necessary downstream distance between the rows - would be essential in more realistic arrays, as they would be made up of several rows making it almost impossible to reach array efficiencies close to 100%.

- Regarding Blockage effects

The results obtained in the configuration 2-3-extra, with a blockage ratio of 12%, show a clear blockage effect produced by the turbines in the first row of the array.

These results match with those obtained in [8] with CFD modelling and shown in figure 18 in section 3.1.1, regarding the flow diversion and acceleration between the array and the walls confining it.

The higher power output of turbine C obtained in configuration 2-3-extra confirms the possibility addressed in [1] of making the most of the increases in the flow speed when the flow is constrained between the array and the headland in real sites (in this case the walls of the flume).

- Regarding wake effects

According to the results obtained and as expected, the wake produced by marine current turbines is a key factor when analyzing interaction between devices.

The velocity recovery profile along the wake at point 0 and its asymptotic character, never reaching the inflow speed again, matches the work done by other researchers.

The persistence of the wake at the other sampled points in the swept area of the rotor, with almost no recovery in the whole distance downstream, could be attributed to an enclosure effect due to the narrowness of the flume.

Some wake rotation was observed by analyzing the change in sign of the x component of the flow speed, however, the very small value of this component and the high turbulence in the flume made it difficult to obtain accurate data.

- Regarding future work

The importance of array effects has been shown in this piece of work and in many other projects carried out during the last few years.

This thesis could be taken by other researchers as a first step to working on experimental models together with numerical models, heading for a better understanding of this technology.

In future work, other researchers and engineers should focus not only on the array effects regarding energy performance and marine current turbine farm exploitation, but also regarding the potential environmental impact of such effects.

7. REFERENCES

[1] L.S. Blunden and A.S Bahaj. Effects of tidal energy extraction at Portland Bill, southern UK predicted from a numerical model. *Proceedings of the 7th European Wave and Tidal Energy Conference*, Porto, Portugal, 2007.

[2] Myers L.E. Operational parameter of horizontal axis marine current turbines, PhD Thesis University of Southampton.

[3] L. Myers, A.S. Bahaj. Simulated electrical power potential harnessed by marine current turbine arrays at the Alderney Race. Sustainable Energy Research Group, University of Southampton, UK, 2004.

[4] J. F. Manwell, J.G. McGowan, A. L. Rogers. Wind Energy Explained, Wiley, 2002.

[5] A.S. Bahaj, L.E. Myers, M.D. Thomson & N. Jorge. Characterizing the wake of horizontal axis marine current turbines. *Proceedings of the 7th European Wave and Tidal Energy Conference*, Porto, Portugal, 2007.

[6] A Technical note on micro-sitting of wind turbines. Centre for Wind Energy Technology.

[7] L. Myers, A.S. Bahaj. Wake studies of a 1/30th scale horizontal axis marine current turbine. Sustainable Energy Research Group, University of Southampton, UK, 2006.

[8] K. Agbeko, S. Love, S. Fitzpatrick. Tidal Stream Power. Energy Systems Research Unit, University of Strathclyde, Glasgow, UK, 2005.

[9] J. Whelan, M. Thomson, J.M.R. Graham, J. Peiro. Modelling of free surface proximity and wave induced velocities around a horizontal axis tidal stream turbine. Imperial College, London

[10] Couch, S., Sun, X., Bryden, I. Modelling of Energy Extraction from Tidal Currents. *Proceedings of the 7th European Wave and Tidal Energy Conference*, Glasgow, UK, 2005.

[11] McCombes, T., MacDonald, M., Hamilton, K., Glynn, J. Marine Current Resource and Technology Methodology. Energy Systems Research Unit, University of Strathclyde, Glasgow, UK, 2006.

[12] Black&Veatch: Phase II UK Tidal Stream Energy Resource Assessment, Carbon Trust, 2005.

[13] Tidal and Current Energy resources in Ireland, Sustainable Energy Ireland, 2006.

[14] Evaluation of Blue Energy Canada Hydro Turbine, H.N. Halvorson Consultants Ltd. Victoria, British Columbia, 1994.

[15] Development, installation and testing of a large-scale tidal current turbine, IT Power, October 2005.

[16] Future Marine Energy, The Carbon Trust, January 2006.

[17] Marine Current Energy Baseload Supply Strategy for Scotland, ESRU, University of Strathclyde, Glasgow, 2005.

[18] Atlas of Marine Renewable Energy Resource, BERR, Department for Business Enterprise and Regulatory Reform, accessed September 2008.

[19] Marine Current Turbines Ltd. Website. www.marinecurrenturbines.com, accessed September 2008.